Master's thesis
Meteorology

Redistribution of meridional atmospheric energy transport caused by polar amplification on an aqua planet

Sándor István Mahó

February 21, 2021

Supervisor: Docent Victoria Sinclair

Examiners: Professor Heikki Järvinen
Docent Victoria Sinclair

UNIVERSITY OF HELSINKI
Master's Programme in Atmospheric Sciences

P.O. Box 64 (Gustaf Hällströmin katu 2)
FI-00014 University of Helsinki

HELSINGIN YLIOPISTO — HELSINGFORS UNIVERSITET — UNIVERSITY OF HELSINKI

Tiedekunta — Fakultet — Faculty	Koulutusohjelma — Utbildningsprogram — Education programme
Faculty of Science	Master's Programme in Atmospheric Sciences

Tekijä — Författare — Author
Sándor István Mahó

Työn nimi — Arbetets titel — Title
Redistribution of meridional atmospheric energy transport caused by polar amplification on an aqua planet

Opintosuunta — Studieinriktning — Study track
Meteorology

Työn laji — Arbetets art — Level	Aika — Datum — Month and year	Sivumäärä — Sidoantal — Number of pages
Master's thesis	February 21, 2021	54 pages

Tiivistelmä — Referat — Abstract

This thesis analyses the alterations of vertically integrated atmospheric meridional energy transport due to polar amplification on an aqua planet. We analyse the energy transport of sensible heat, latent energy, potential energy and kinetic energy. We also cover the energy flux of the mean meridional circulation, transient eddies and stationary eddies. In addition, we also address the response of the zonal mean air temperature, zonal mean zonal wind, zonal mean meridional wind, zonal mean stream function and zonal mean specific humidity.

Numerical model experiments were carried out with OpenIFS in its aqua planet configuration. A control (CTRL) and a polar amplification (PA) simulation was set up forced by different SST (sea surface temperature) patterns.

We detected tropospheric warming and atmospheric specific humidity increase 15-90° N/S and reduction of the meridional temperature gradient throughout the troposphere. We also found reduced strength of the subtropical jet stream and slowdown of the mean meridional circulation. Important changes were identified in the Hadley cell: the rising branch shifted poleward and caused reduced lifting in equatorial areas.

Regarding the total atmospheric vertically integrated meridional energy transport, we found reduction in case of the mean meridional circulation and transient eddies in all latitudes. The largest reduction was shown by the Hadley cell transport (-15%) and by midlatitude transient eddy flux (-23%). Unlike most studies, we did not observe that meridional latent energy transport increases by polar amplification. Therefore, it is stated that the increased moisture content of the atmosphere does not imply increased meridional latent energy transport, and hence there is no compensation for the decrease of meridional dry static energy transport. Lastly, we did not detect stationary eddies in our simulations which is caused by the simplified surface boundary (i.e. the water-covered Earth surface). The main finding of this thesis is that polar amplification causes decreasing poleward energy transport on an aqua planet.

Avainsanat — Nyckelord — Keywords
Polar amplification, meridional energy transport, aqua planet simulations, OpenIFS

Säilytyspaikka — Förvaringsställe — Where deposited

Muita tietoja — övriga uppgifter — Additional information

Contents

1. Introduction

Contemporary climate change makes our society address several questions arising from the high uncertainty of climatic, economic and social effects of the phenomenon. From a scientific point of view, it is still under intense debate how the climate system reacts to anthropogenic forcing particularly induced by greenhouse gas emissions. Recent global trends (Pachauri et al., 2014) show accelerating surface warming, however, the magnitude of surface temperature change shows regional differences.

Polar regions are of particular interest, since both observed and predicted surface temperature increase is enhanced in these areas (Serreze and Barry, 2011; Smith et al., 2019). For example, the observed zonal average warming in the Arctic is more than twice as large as in midlatitude areas and more than three times large as in tropical regions based on the National Aeronautics and Space Administration Goddard Institute for Space Sciences (NASA GISS) temperature analysis between 1970 and 2019 (Appendix A). Therefore, the phenomenon is often referred as polar amplification, since polar areas experience excessive surface temperature increase resulting in severe feedback mechanisms not only in the climate system, but also in the ecosystem (Post et al., 2013). Polar amplification is also a significant feature of CMIP5 ensemble global climate model projections for the future (Smith et al., 2019), especially those experiments which were run under high emission scenarios (e.g. RCP 8.5). Thus, in the future polar warming is expected to continue and become even stronger (Pachauri et al., 2014).

The Polar Amplification Model Intercomparison Project (PAMIP) within the 6th Coupled Model Intercomparison Project (CMIP6) is currently seeking for answers for the causes and effects of polar amplification by systematic climate model experimental design (Smith et al., 2019). Here, it is worth emphasizing that not only the causes but also the consequences of polar amplification are still highly uncertain, especially in terms of atmospheric general circulation response.

To understand the alterations in the atmosphere, it is recommended to carry out climate simulations with full Atmospheric General Circulation Models (AGCMs) including complex orography, and simulations under idealized set-ups. The aqua planet framework proposed by Neale and Hoskins (2000) is an example of the latter one which can be used as a benchmark for AGCMs (Blackburn and Hoskins, 2013). Aqua planet models lie between complex AGCMs and less complex idealized moist core models in the modelling hierarchy proposed by Blackburn and Hoskins (2013). Aqua planet models simulate atmospheric processes on an idealised water-covered Earth including interactions with latent heat, clouds and radiative feedbacks under simplified surface boundary conditions (i.e. in the absence of continents) (Shaw et al., 2016). Furthermore, aqua planet models are able to reflect the circulation response (e.g. Hadley circulation response, extratropical storm track response) to changes in sea surface temperature (SST) gradients (Blackburn and Hoskins, 2013; Shaw et al., 2016).

As it was mentioned earlier, currently it is under debate how the atmospheric general circulation reacts to polar amplification including changes in meridional energy transport (Smith et al., 2019). It is known that atmospheric meridional energy transport is driven by the differences in net radiative energy between the tropics and the poles (Hartmann, 2016). By polar amplification, there are two opposing mechanisms which affect meridional energy transport. If surface temperature increases in polar areas, the Equator-to-Pole temperature gradient decreases which

reduces atmospheric dry energy transport. On the other hand, atmospheric moisture transport is expected to increase by polar warming, which offsets the effect of the meridional temperature gradient, since it strengthens latent energy transport (Manabe and Wetherald, 1980; Hwang et al., 2011). In addition, it is also unknown how midlatitude eddies adjust to polar amplification regarding eddy heat flux and eddy kinetic energy (Yuval and Kaspi, 2020). Therefore, it is worth studying the above mentioned processes through different model configurations.

For this study, an AGCM (i.e. OpenIFS, for details see Section 3.1) configured as an aqua planet was used to study the atmospheric circulation response to polar SST increase in terms of energy transport. The aims of this thesis are the following:

- to quantify how the zonal and time mean temperature, zonal wind, meridional wind, specific humidity and mass stream function reacts to polar amplification on an aqua planet,

- to inspect how atmospheric meridional energy transport reacts to polar amplification on an aqua planet by **i)** quantifying the zonal and time mean vertical integrals of meridional energy transport of total atmospheric energy, sensible heat, latent energy, potential energy and kinetic energy and by **ii)** quantifying the contribution of mean meridional circulation, transient eddies and stationary eddies to zonal and time mean vertical integrals of meridional total atmospheric energy transport, sensible heat transport, latent energy transport, potential energy transport and kinetic energy transport.

2. Background

2.1 Overview of atmospheric general circulation

The general circulation of the atmosphere is a global system of atmospheric motions which is primarily driven by the uneven distribution of solar energy between different latitudes. It is largely responsible for transporting heat and moisture from tropical regions towards the poles and it also induces ocean circulation by surface wind stress (Hartmann, 2016). It is worth emphasizing that poleward energy transport is a general feature of the general circulation. Changes in the mean state of the atmosphere could result in dramatic changes in the circulation system (Yuval and Kaspi, 2020). In this section basic features of the general circulation are summarized with special focus on the zonal-mean circulation and the eddy circulation.

2.1.1 Observed mean state of the atmosphere

This section includes basic statistics of atmospheric variables derived from observations based on the works of Oort and Rasmusson (1970); Peixoto and Oort (1992). The figures used for representing the basic atmospheric state are obtained from ERA-40 reanalysis database (*ERA-40 Atlas*, n.d.).

The temperature distribution is considered being a fundamental property of the atmosphere, since it reflects the wind structure and the thermodynamic state of the atmosphere (Peixoto and Oort, 1992). Fig. 2.1 illustrates the annual mean

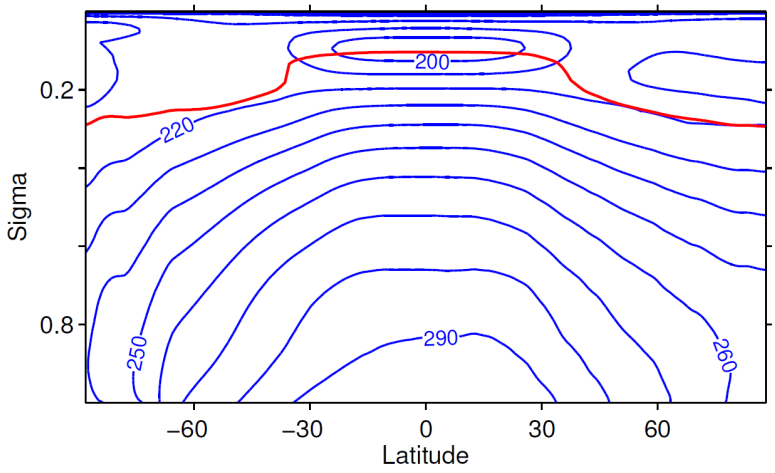

Figure 2.1: Zonal-mean cross section of annual mean temperature (K) in sigma (σ) coordinates from ERA-40 database. The red line illustrates the tropopause. Figure adopted from O'Gorman (n.d.).

temperature distribution as a function of latitude and altitude. According to Fig. 2.1, time averaged tropospheric temperature decreases with height and with latitude. In addition, the largest meridional temperature gradient occurs in midlatitudes in the middle troposphere (700 hPa/0.7σ). The height of the tropopause falls towards higher latitudes (see red line on Fig. 2.1). In the lower stratosphere the temperature gradient is reversed, because the lowest temperatures are observed over the tropics as a result of high tropopause height. Lower-tropospheric meridional temperature gradient is of interest, because it is associated with the strength of zonal mean flow and baroclinity. It has also a major effect on the intensity of poleward energy transport.

The temperature variability can be analysed in space and time. Time variations on a timescale of days to some weeks are mainly associated with transient eddies (for details see Section 2.1.4). As an example, Fig. 7.9b from Peixoto and Oort (1992) showing the day-to-day standard deviation of temperature reveals that temperature variations are predominant in midlatitude regions. Similarly, the east-west standard deviation of temperature (Fig. 7.9c from Peixoto and Oort (1992))

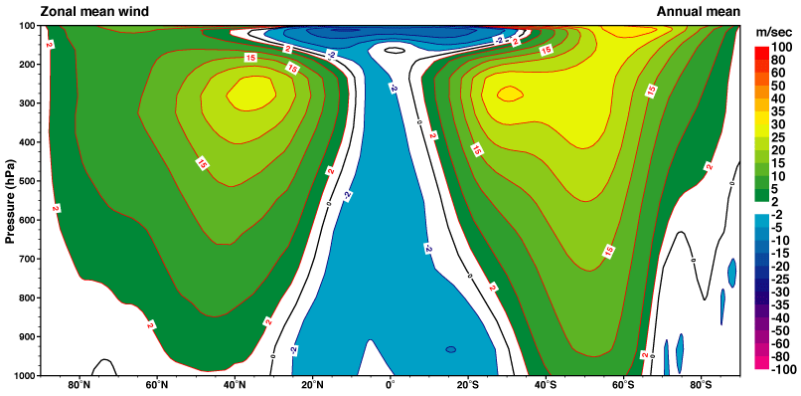

Figure 2.2: Zonal mean cross-section of annual mean u-wind ($m\ s^{-1}$) from ERA-40 (*ERA-40 Atlas*, n.d.).

peaks at midlatitude regions associated with standing waves (for details see Section 2.1.5). The smallness of the Coriolis parameter in tropical areas renders temperature variations minor.

The zonal mean zonal wind field (u component of the wind), that is demonstrated by Fig. 2.2, is closely related to the global temperature distribution. Surface winds tend to be westerly in midlatitudes and easterly in the tropics satisfying angular momentum balance of the Earth (Oort and Peixóto, 1983). Westerly winds reach their maxima close to the tropopause at 35°. These circumpolar winds are generally referred as subtropical jet streams, which are resulted from the effect of conservation of angular momentum and thermal wind law. Thermal wind law (Eq. 2.1) states that vertical wind shear ($\partial u_g/\partial p$) is a function of meridional temperature gradient ($\partial T/\partial y$). In Eq. 2.1 u_g, R_d, f_0, p and T denotes the zonal geostrophic wind, the gas constant for dry air, the Coriolis parameter, the pressure and the temperature respectively. According to Eq. 2.1, high-level winds intensify by steeper meridional temperature gradients.

$$\frac{\partial u_g}{\partial p} = \frac{R_d}{p f_0} \frac{\partial T}{\partial y} \tag{2.1}$$

Variations in the zonal mean circulation are also important to point out since

they reflect the atmospheric eddy activity. The corresponding figures describing this phenomenon are Fig. 7.20b and Fig. 7.20d from Peixoto and Oort (1992). Temporal zonal wind variations on a daily timescale are similar to temperature variability having a maximum at 50°. Meridional variations in the zonal wind has smaller magnitude and has local maximum values in midlatitude areas associated with standing waves and the jet streams (i.e. subtropical and polar jet stream).

2.1.2 Decomposition of atmospheric circulation

As it was highlighted in the previous section, meteorological fields that describe the state of the atmosphere change substantially both in time and space. Therefore, it is convenient to define statistics concerning variations in space, in time and in space-time domain. The following decomposition approach is based on Peixoto and Oort (1992). First, the zonal mean of variable s is presented in the following way:

$$[s] = \frac{1}{2\pi} \int_0^{2\pi} s \; d\lambda \tag{2.2}$$

where $[s]$ denotes the zonal mean of variable s over a latitude circle and λ stands for longitude. The deviation from zonal mean of variable s (s^*) is shown by Eq. 2.3. It is clear, that the sum of zonal mean and the deviation from zonal mean gives the total quantity of s.

$$s^* = \; s - [s] \tag{2.3}$$

The same approach can be obtained in time. Eq. 2.4 denotes for the time mean of s ($\bar{s}$) by integrating s over a specific time period ($t_2 - t_1$).

$$\bar{s} = \frac{1}{t_2 - t_1} \int_{t_1}^{t_2} s \; dt \tag{2.4}$$

The deviation from time mean (s', Eq. 2.5) is obtained in a similar way as s^*.

$$s' \; = \; s - \bar{s} \tag{2.5}$$

Combining space and time equations (Eq. 2.3 and Eq. 2.5) one can prove that variable s corresponds to the sum of zonal and time mean of s ($[\bar{s}]$), the zonal deviation from time mean of s ($\bar{s}^*$) and the deviation from time mean of s (s') shown by Eq. 2.6.

$$s = [\bar{s}] + \bar{s}^* + s' \tag{2.6}$$

By studying the atmospheric general circulation, we are interested in the variance of one variable and the covariance of different variables. Eq. 2.7 and Eq. 2.8. gives the time variance of variable s and the time covariance of variables s and q respectively. Note, that the same can be done in space which is not shown here.

$$\overline{s'^2} = \frac{1}{t_2 - t_1} \int_{t_1}^{t_2} (s - \bar{s})^{\,2} dt \tag{2.7}$$

$$\overline{s'q'} = \frac{1}{t_2 - t_1} \int_{t_1}^{t_2} (s - \bar{s})\,(q - \bar{q})\,dt \tag{2.8}$$

The zonal and time mean product of variable s and q ($[\overline{sq}]$) is given by Eq. 2.9, where the different terms on the right-hand side (RHS) represent the mean meridional circulation, the effect of stationary eddies and the effect of transient eddies respectively.

$$[\overline{sq}] = [\bar{s}]\,[\bar{q}] + [\bar{s}^*\bar{q}^*] + \left[\overline{s'q'}\right] \tag{2.9}$$

The subsequent sections give deeper analysis of the above mentioned circulation elements.

2.1.3 Mean meridional circulation

The mean meridional circulation (shortly MMC) consists of the zonal and time mean meridional and vertical wind ($[\bar{v}]$ and $[\bar{\omega}]$ respectively). Their combined effect can be described by the mass stream function (ψ, Eq. 2.10) which gives the northward mass flux (in $kg\ s^{-1}$) above a selected pressure level (p) (Hartmann, 2016).

$$\psi\,(p) = \frac{2\pi a \cos\phi}{g} \int_0^{p_0} [\bar{v}]\,dp \tag{2.10}$$

In Eq. 2.10 g and ϕ stands for the gravity constant and latitude respectively. The mean meridional wind is proportional to the vertical gradient of the mass stream function (Eq. 2.11) and the mean vertical wind is proportional to the latitudinal changes of the mass stream function (Eq. 2.12).

$$[\bar{v}] = \frac{g}{2\pi a \cos\phi}\frac{\partial\psi}{\partial p} \tag{2.11}$$

$$[\bar{\omega}] = -\frac{g}{2\pi a^2 \cos\phi}\frac{\partial\psi}{\partial\phi} \tag{2.12}$$

The vertical cross-section of the annual mass stream function is apparent from Fig. 2.3, where the three-cell regime of the MMC is clearly visible. The figure also reveals that the observed circulation is approximately symmetric about the equator in terms of annual mean, however, the mean ascent associated with the ITCZ (i.e. Intertropical Convergence Zone) is slightly shifted to north. By eliminating the effects of land-ocean distribution (i.e. circulation on an aqua planet) the MMC would be closer to symmetry between the two hemispheres. The strongest meridional overturning occurs in the tropical Hadley cell (0-35°) which is a thermodynamically direct circulation: warm air transported by the surface trade winds rises at the equator and cold air sinks at the subtropics as part of the compensating subsidence (Hartmann, 2016). The Ferrel cell (35-65°) shows a moderate meridional overturning with half of the strength of the Hadley cell. The Ferrel cell, which is generated by midlatitude eddies (Holton, 1973) is a thermodynamically indirect circulation, since warm air sinks at the subtropics and cold air rises at the edge of polar areas. The thermodynamically direct polar cell shows a very weak meridional mass flux compared to the Hadley cell. The mean meridional circulation is an important component of the atmospheric circulation, however, the role of eddies in midlatitude regions surpasses the effect of MMC. The description of eddies is outlined in the following sections.

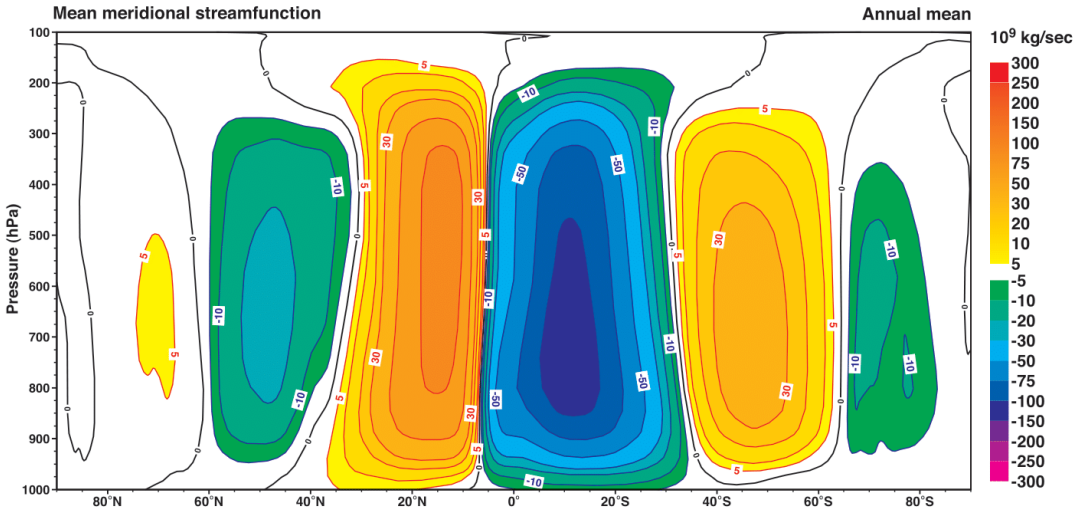

Figure 2.3: Mass stream function for the annual mean based on ERA-40 reanalysis (*ERA-40 Atlas*, n.d.).

2.1.4 Transient eddies

Stemming from the temporal variations of the flow, transient eddy fluxes are associated with eastward moving weather disturbances which are clearly visible on weather charts (Hartmann, 2016). These disturbances are caused and maintained by baroclinic instability, which is due to the existence of the low-level temperature gradient (Holton, 1973). The structure of eddies gives evidence of positive correlation between meridional velocity (v), temperature (T) and specific humidity (q) fluctuations. Since the geopotential height (Z) wave is located downstream of the temperature (T) wave, eddy heat flux ($[T^*v^*]$) and moisture flux ($[q^*v^*]$) are positive. [1] This can be followed by Fig. 2.4 which displays the typical structure of midlatitude waves (in the Northern Hemisphere) showing the Z field (corresponding to streamlines of the geostrophic wind) and the T field. It is apparent, that warm air advection ($T^* > 0$) is associated with northward flow ($v^* > 0$) and cold air

[1] Note that moisture field tend to follow the temperature field. Also note that s^*v^* here means the total eddy flux of variable s.

advection ($T^* < 0$) is associated with southerly flow ($v^* < 0$) resulting in a decrease in the heat difference between the poles and the tropics.

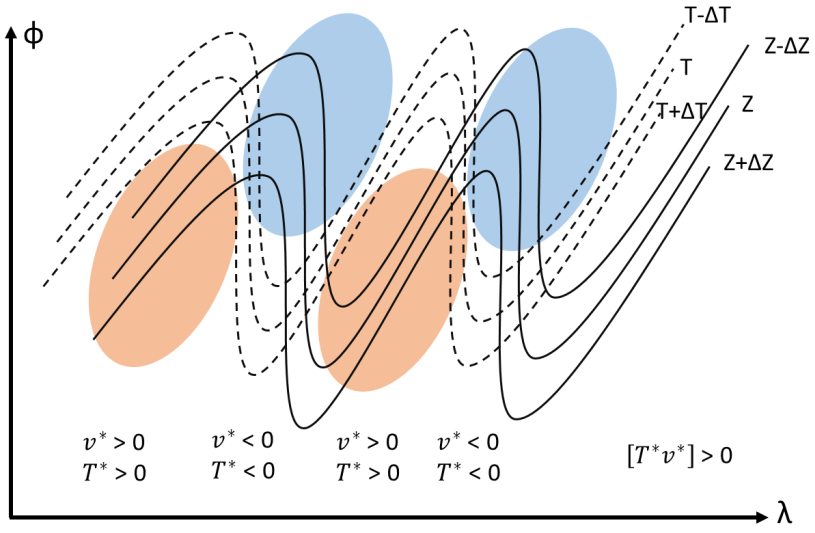

Figure 2.4: Schematic of the structure of midlatitude baroclinic waves on a horizontal plane (λ, ϕ). Solid and dashed lines show the geopotential and the temperature wave respectively. Coloured patches show areas of warm (red) and cold air (blue). Below, temperature (T) and meridional wind (v) tendencies are displayed. Based on Hartmann (2016).

2.1.5 Stationary eddies

Stationary eddies (or standing waves) are associated with the longitudinal variation of the time averaged flow. In other words, these patterns refer to the departure of time average from zonal symmetry (Hartmann, 2016). The most important wave type in terms of driving large-scale meteorological processes is called planetary Rossby-wave which is a potential vorticity conserving motion stemming from the so-called β-effect. The β-effect is the variation of Coriolis parameter with latitude (Holton, 1973). Planetary waves can be generated by topographic forcing of large mountain ridges or by longitudinally dependent diabatic heating (e.g. West Pacific Warm Pool) (Holton, 1973). The latter can result from the irregular distri-

bution of continents and oceans, or from thermal contrasts between warm and cold ocean waters (Hartmann, 2016). Stationary waves play a major role in controlling weather in midlatitudes and contributing to meridional energy transport. They tend to act against the imbalance of heat arising from the insolation differences between latitudes by forcing cold, surface polar air to move equatorward and warm tropical air to move poleward (Oliver, 2008). They have maximum heat transport in low levels, since the phase difference between pressure and temperature are largest in lower levels (see Fig. 2.4 for a typical midlatitude wave pattern; Hartmann (2016)).

Ideally, in aqua planet simulations stationary eddies do not appear since the forcing factors are missing (i.e. orography, land-sea distribution) (Feldl et al., 2017).

2.2 Energy in the atmosphere

2.2.1 Forms of atmospheric energy

The atmosphere contains different amount of energy in different forms, namely internal energy (Eq. 2.13), potential energy (Eq. 2.14), latent energy (Eq. 2.15) and kinetic energy (Eq. 2.16).

$$E_{int} = C_v T \tag{2.13}$$

$$E_{pot} = gZ \tag{2.14}$$

$$E_w = Lq \tag{2.15}$$

$$E_{kin} = k = \frac{1}{2}\left(u^2 + v^2 + w^2\right) \approx \frac{1}{2}\left(u^2 + v^2\right) \tag{2.16}$$

In equations 2.13-2.16 C_v refers to atmospheric specific heat at constant volume ($J\ kg^{-1}\ K^{-1}$), g is gravitational acceleration ($m\ s^{-2}$), L is latent heat for vaporiza-

tion ($J\ kg^{-1}$) and w is the vertical wind ($m\ s^{-1}$). Note that k denotes for kinetic energy

In the equation of meridional atmospheric energy transport (Eq. 2.18 in the next section) atmospheric entalphy is used as representing sensible heat (instead of internal energy). The expression for atmospheric entalphy is shown by Eq. 2.17 where C_p refers to isobaric atmospheric specific heat ($J\ kg^{-1}\ K^{-1}$).

$$E_{P^+} = C_p T \tag{2.17}$$

Atmospheric enthalpy can be generated by diabatic heating (i.e. by radiation, condensation heating, sensible heat flux, etc.). Latent energy is usually formed by evaporation and lost by condensation. Kinetic energy is created from available potential energy for instance when warm air ascends and cold air sinks (i.e. Hadley circulation, midlatitude eddies) and it is lost by frictional dissipation. The most important forms of energy are internal, potential and latent energy contributing to 70.4%, 27.1% and 2.5% to the total energy respectively (Oort and Peixóto, 1983). The contribution of kinetic energy to total atmospheric energy is small compared to the other energy forms, however, kinetic energy is crucial for atmospheric circulation and energy redistribution (Oort, 1971; Oort and Peixóto, 1983; Peixoto and Oort, 1992). Energy transfer between the various forms occurs constantly in the atmosphere. Furthermore, energy is continuously transported between different latitudes by different transport modes (i.e. mean meridional circulation and eddies) on average from the tropics towards the poles which is the main topic of the consecutive section.

2.2.2 Atmospheric energy transport

Energy transport in the globe takes place both in horizontal and in vertical direction. Energy transport is carried out by atmospheric and oceanic motions. Fundamentally, the atmospheric component exceeds oceanic energy transport. Meridional

energy transport is of particular interest, since it is responsible for balancing the net incoming energy differences between low and high latitudes. Total meridional atmospheric energy transport includes fluxes of sensible heat, latent heat, potential energy and kinetic energy. Zonal mean vertically integrated total energy transport (Fig.13.11a from (Peixoto and Oort, 1992)) is poleward everywhere on the planet having a maximum at 60°N. Peak season of total energy transport are winter months on each hemisphere. Vertically integrated sensible and latent heat transport is primarily determined by the direction of surface winds, since they have maximum in the lower troposhere. Vertically integrated potential energy transport is concentrated in the upper troposphere and its sign is reversed compared to the flow of sensible heat. Predominantly, the mean meridional circulation is the most important transport mode of potential energy. Kinetic energy is essentially located in the higher troposphere due to higher wind velocities and it is mostly driven by the mean meridional circulation and transient eddies (Peixoto and Oort, 1992).

Decomposition of meridional energy transport

Atmospheric meridional energy transport encompasses all energy forms shown earlier and it can be decomposed into the contributions of mean meridional circulation (MMC), stationary eddies (SE) and transient eddies (TE). The total meridional energy flux across a latitude is presented by Eq. 2.18 together with the energy components decomposed into the above mentioned three circulation components (i.e. terms in the square bracket). The presented approach is equivalent with the work of Oort and Peixoto (1983) where they investigated the conditions for global energy balance. Note, that meridional energy transport at a specific latitude circle (ϕ) is the vertically integrated energy flux throughout the whole atmosphere composed of sensible heat (C_pT), potential energy (gZ), latent heat (Lq) and kinetic energy transport (k). In Eq. 2.18, $\bar{F}$ represents the mean energy flux at a latitude

circle, a is the Earth's radius and the integral represents the vertically integrated total atmospheric energy flux. In Eq. 2.18 LHS (left hand side) shows the total meridional energy transport which is decomposed into the energy flux by the mean meridional circulation ($\bar{F}\,(MMC)$), by transient eddies ($\bar{F}\,(TE)$) and by stationary eddies ($\bar{F}\,(SE)$). The components of the energy transport (i.e. the squared bracket in Eq. 2.18) is highlighted and decomposed into the contribution of the above mentioned circulation components expressed in the curly brackets. The detailed derivation of this formula can be found in Peixoto and Oort (1992), Chapter 13.

$$\bar{F} = 2\,\pi\,a\,\cos(\phi)\int_0^{p_0}\left[\overline{v\,(C_pT + gZ + Lq + k)}\right]\frac{dp}{g} = \bar{F}\,(MMC) + \bar{F}\,(TE) + \bar{F}\,(SE)$$

$$\begin{aligned}\left[\overline{v\,(C_pT + gZ + Lq + k)}\right] &= \left\{C_p\,[\bar{v}]\left[\bar{T}\right] + g\,[\bar{v}]\left[\bar{Z}\right] + L\,[\bar{v}]\,[\bar{q}] + [\bar{v}]\left[\bar{k}\right]\right\} \\ &+ \left\{C_p\left[\overline{v'T'}\right] + g\left[\overline{v'Z'}\right] + L\left[\overline{v'q'}\right] + \left[\overline{v'k'}\right]\right\} \\ &+ \left\{\left[\bar{v}^*\bar{T}^*\right] + g\left[\bar{v}^*\bar{Z}^*\right] + L\,[\bar{v}^*\bar{q}^*] + \left[\bar{v}^*\bar{k}^*\right]\right\}\end{aligned} \tag{2.18}$$

Observed decomposed meridional energy transport

Total atmospheric energy content peaking at low latitudes stimulates poleward energy transport. However, the sign and the quantity of meridional energy transport varies considerably between the different circulation components and between the different energy forms as well. In the subsequent paragraphs energy transport by the mean meridional circulation and eddies is written in detail which is followed by a brief summary. The corresponding figures revealing the decomposed meridional energy transport are Fig.13.5-13.9 from Peixoto and Oort (1992).

The mean meridional circulation (first curly bracket RHS in Eq. 2.18) transports energy by a three-cell regime in both hemispheres having maximum transport

in the Hadley cell. The tropical Hadley cell transports sensible and latent heat towards the equator and it transports potential energy towards the poles. In the rising branch close to the equator heat is converted to potential energy and air cools (Oort, 1971). Here condensational heating by Cumulus towers is balanced by adiabatic cooling (Webster, 2004). In the upper flow, potential energy is displaced to the subtropics where this relatively cold air becomes warm again by the sinking branch of the Hadley cell (i.e. adiabatic warming). In this sense, potential energy is converted back to internal energy. This cycle cools the atmosphere close to the equator and warms it at the subtropics leading to more significant meridional temperature gradient in midlatitude areas (Oort, 1971; Webster, 2004). In the indirect Ferrel cell, sensible and latent heat is transported towards the poles by the northwesterly mean surface winds and potential energy is transported towards lower latitudes by the upper branch of the cell. Kinetic energy transport by the MMC is a function of the mean wind in the upper troposhere. Convergence of mean kinetic energy occurs at regions where subtropical jets are located (30°) having poleward flux by the upper branch of the Hadley cell and equatorward flux by the upper branch of the Ferrel cell. The polar cell has similar energy transport pattern to the Hadley cell, however, the fluxes are quite modest (Oort, 1971; Oort and Peixóto, 1983; Hartmann, 2016).

Eddies receiving their energy from the mean flow transport massive amounts of energy poleward (Holton, 1973; Webster, 2004). Their effect is more prominent during the local winter of a hemisphere (Peixoto and Oort, 1992). It is also a rather significant feature of the eddy energy transport that the contribution of stationary eddies (third curly bracket RHS in Eq. 2.18) is considerably smaller than the contribution of transient eddies (second curly bracket RHS in Eq. 2.18; Peixoto and Oort (1992)). Eddies transport sensible and latent heat poleward in the lower and middle troposphere peaking at 35° and 50° respectively. It important to note that these fluxes are higher than the fluxes by the Ferrel cell (Oort and Peixóto, 1983;

Hartmann, 2016). Potential energy transport by eddies is negligible, however equatorward transport by transient eddies at the subtropics is of interest since they can provide energy source for tropical disturbances such as ENSO (El Niño - Southern Oscillation) (Mak, 1969; Oort and Peixóto, 1983; HSU et al., 2009). Transport of eddy kinetic energy is poleward between 15° and 60°, and it is equatorward in latitudes higher than 60° which defines a convergence center of eddy kinetic energy. This convergence center is located at 60° and it is associated with the zonal fluctuations of the eddy-driven jet (Oort, 1971; Oort and Peixóto, 1983).

To sum up, it is observed that the vast majority of atmospheric energy is transported by the mean meridional circulation and by transient eddies. The energy transport by the mean meridional circulation is most important in lower latitudes, where the flux by the Hadley cell is more or less equal with the total energy transport. Potential energy transport is the most important energy component in case of MMC which causes that the total energy flux by the Hadley cell is poleward even though sensible and latent heat is transported to the equator. In midlatitude areas, transient eddy energy flux is the predominant energy transport mode which carries high amounts of sensible and latent heat towards the poles. Stationary eddies are mainly apparent in midlatitude areas, however their contribution to meridional energy transport is small.

2.3 Polar amplification: causes & consequences

According to the definition of the Polar Amplification Model Intercomparison Project (PAMIP) of CMIP6 polar amplification occurs when external radiative forcing produces a larger surface temperature change at high latitudes than global average (Smith et al., 2019). In this section the physical processes that drive this phenomenon and the possible effects on global climate is discussed briefly.

2.3.1 Theories for the cause of polar amplification

Polar amplification is a common feature of global climate model simulations for the future which was highlighted in the 5^{th} Assessment Report of the IPCC (Pachauri et al., 2014). Figure 2.5 presents the average change in surface temperature based on multi-model mean projections for 2081-2100 under RCP 2.6 and RCP 8.5 emission scenarios. The graph reveals a clear trend of enhanced surface temperature warming in polar areas (especially in the Northern Hemisphere) in response to anthropogenic greenhouse gas emissions in case of both emission scenarios. Polar amplification also appears in observations and in reanalysis products, particularly in the Arctic, therefore, it is often referred as Arctic Amplification (Hansen et al., 2010; Screen and Simmonds, 2010). In addition, paleoclimate simulations perturbed by CO_2 also shows evidence for this phenomenon (Lee, 2014; Masson-Delmotte et al., 2013). Polar amplification has become an increased focus of recent climate research aiming to detect the driving factors and the possible consequences regarding the Earth system which are still uncertain (Pithan and Mauritsen, 2014; Smith et al., 2019).

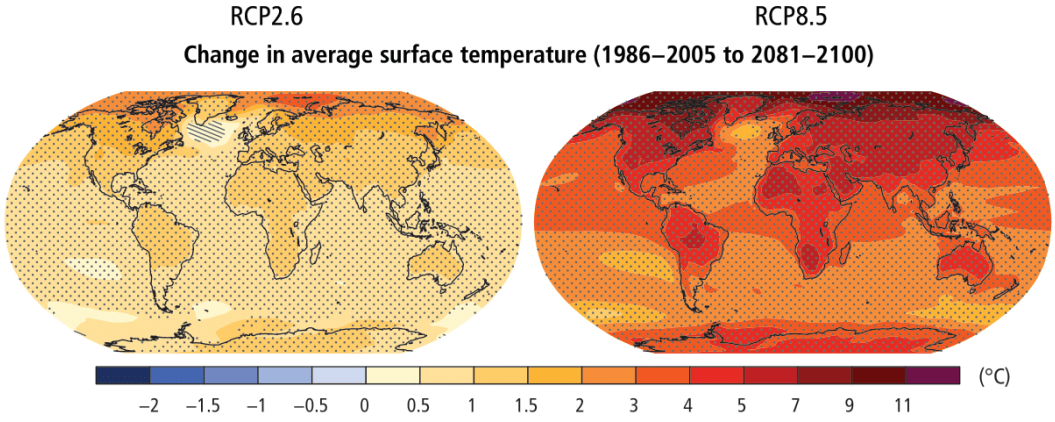

Figure 2.5: Global change in surface temperature based on multi-model mean ensembles projections for 2081-2100 relative to 1986-2005 according RCP 2.6 (left) and RCP 8.5 (right). Figure adopted from Pachauri et al. (2014).

Feedback mechanisms are crucially important for the process of polar amplification (Pithan and Mauritsen, 2014; Smith et al., 2019). It is widely known that the surface albedo feedback is one of the causing mechanisms of the phenomenon, however, its relative importance is still the topic of debate (Pithan and Mauritsen, 2014). The abovementioned theory states that the retreating highly reflective polar ice and snow regions increase the amount of absorbed solar radiation which in turn warms these areas. However, it was shown by climate simulations that the surface albedo feedback alone is unable to explain polar amplification (Hall, 2004; Graversen and Wang, 2009).

According to Pithan and Mauritsen (2014), the Planck and the lapse rate feedbacks are particularly important. The Planck feedback states that an external forcing is balanced by higher temperature increase at colder latitudes (poles) than at warmer latitudes (tropics). This statement can be simply understood by the Stefan-Boltzmann radiation law, which states that a given increase in emitted radiation requires a larger temperature increase at colder background temperatures (i.e. emitted radiation is proportional to the fourth power of absolute temperature of a blackbody).

The lapse rate feedback is related to the vertical temperature profile of the atmosphere which is negative at the tropics but positive at high latitudes. In the tropics surface warming causes increased convective activity and therefore increased condensation heating in the upper troposphere decreasing the environmental lapse rate. Upper tropospheric warming relative to the lower parts induces stronger longwave cooling and therefore a negative feedback to surface warming (Stocker, 2011). In polar areas, warming is restricted to the lower troposphere due to stability conditions (Bintanja et al., 2012) leading to a steeper lapse rate which causes imbalance of TOA (top of the atmosphere) radiation. This imbalance can be offset by larger surface temperatures, meaning a positive feedback on surface warming (Pithan and

Mauritsen, 2014). Other feedbacks, such as the cloud feedback, the water vapour feedback can be also important for polar amplification (Smith et al., 2019).

Increased atmospheric meridional moist energy transport is also a suggested mechanism for polar amplification, leading to energy flux convergence at the poles resulting in polar warming (Manabe and Wetherald, 1980; Smith et al., 2019). A general circulation-based mechanism for polar amplification was also suggested by Lee (2014), which indicates that large-scale localized tropical heating induce poleward propagating Rossby-wave trains that transport moisture and heat towards the poles. The theory was supported by some evidence from paleoclimate proxy (Stott et al., 2002; Visser et al., 2003; Lee, 2014) and recent trends of tropical convection (Flournoy et al., 2016; Clark and Lee, 2019), however, further research is needed to confirm this theory (Lee, 2014). Lastly, internal variability of the atmosphere may have an effect on polar warming trends as well, which can be characterized by namely the Northern Annular Mode (NAM) and the Southern Annular Mode (SAM, Smith et al. (2019)).

2.3.2 Effects of polar amplication on climate

Polar warming has a major effect on melting of polar ice sheets, changes in oceanic and atmospheric circulation and carbon uptake at polar oceanic regions (Smith et al., 2019). Atmospheric circulation changes due to polar warming is an active research area with many contradictory results. Recent observations show spatial differences in climatic trends in polar areas, such as persistent and extreme cold winter weather (i.e. cold spell) in Eurasia and North America. The phenomenon is often referred as warm Arctic and cold continents pattern, which is caused by frequent blockings situations (Liu et al., 2012; Mori et al., 2014; Smith et al., 2019). However, these trends can be caused by the internal variability of the atmosphere. Therefore, numerical model experiments are crucially important for detecting the

relationship between polar amplification and changes in the climate system (Smith et al., 2017, 2019).

From the aspect of general circulation, it is known that the meridional temperature gradient decreases with the degree of polar amplification in the lower/middle troposphere. This could potentially cause weakening of midlatitude storm tracks and negative tendency in NAO (Smith et al., 2019). However, according to simulations by Smith et al. (2017) the storm track response is highly dependent on the local background state of the atmosphere. It is also hypothesized that polar warming can moisten the atmosphere leading to increased release of latent heat and therefore precipitation increase in polar areas (Singarayer et al., 2006). The jet stream response to polar amplification is also controversial, however, some authors agree that the dwindling low-level Equator-to-Pole temperature gradient fosters the oscillation of the polar jet stream resulting increasing number of blocking situations (Meleshko et al., 2016; Smith et al., 2019). In terms of oceanic circulation, there is evidence that polar amplification causes weakening of Atlantic Meridional Overturning Circulation (AMOC) which decreases the meridional oceanic heat transport (Sévellec et al., 2017) and gives rise to growing number of winter storms (Jackson et al., 2015). In addition, the unequal rate of warming between the two hemispheres can possibly shift the ITCZ northward which affects tropical storm activity and rainfall rate in the Sahel region (Smith et al., 2017, 2019).

3. Methods

3.1 OpenIFS

Numerical model simulations were carried out using OpenIFS which is a global numerical weather prediction model developed by the European Centre for Medium-Range Weather Forecasts (ECMWF). OpenIFS is available for research and academic institutions under license from 2013, and it provides a similar capacity for forecasting as IFS (Integrated Forecast System), however, it does not include a data assimilation system. The dynamical core, the physical parameterisation schemes, the land surface model and the ocean wave model are the same as in full IFS. Without data assimilation scheme, OpenIFS can be only used with externally generated initial conditions. OpenIFS has been used as a training tool in academic teaching (Szépszó et al., 2019). Moreover, it has been applied for several research topics including understanding the evolution of high impact cyclones (e.g. Laurila et al. (2020), Rantanen et al. (2020)) and climate change projections under idealised setups (e.g. Sinclair et al. (2020)). Details of the model can be found in the official site (*OpenIFS Documentation*, n.d.). For this research Cy43r3 version of the model was used which was operational at ECMWF from July 2017 to June 2018 (*IFS Cycle 43 r3*, n.d.).

3.2 Experimental setup and data

The model was configured as an aqua planet with prescribed SST (sea surface temperature) distributions. In aqua planet models the entire surface is covered by an ocean, therefore they do not include orography. The prescribed SST fields were held constant throughout the simulations. Two simulations were carried out: a control simulation (CTRL) and a polar amplification experiment (PA). Both simulations were run at a resolution of T255 and with 60 model levels. The grid spacing was 0.703° (equivalent to 78 km). The model top level was located at 10 hPa. Each of the simulations were run for 11 years. The first year of each simulation was excluded from the analysis in order to guarantee that the model reached equilibrium. According to Sinclair et al. (2020) the model reaches a balanced state within a year under a similar configuration. Therefore, omitting the first-year output data ensures that the analysis covers only steady-state conditions. For the data analysis, 5 years of output data has been processed (i.e. from simulation year 2 to 6). In addition, both experiments were run with a diurnal cycle of incoming solar radiation. Seasonal cycle was not incorporated into the simulations. Instead, the incoming solar radiation was fixed at equinoctial value resulting in a symmetric distribution about the equator. Sea ice simulations and ocean dynamics were also not incorporated into the numerical model experiments. In the following, details of the two experiments are presented.

3.2.1 Control (CTRL) simulation

The CTRL simulation was forced by a zonally uniform SST field which was proposed by Neale and Hoskins (2000). This SST field follows the QObs distribution (for details see Neale and Hoskins (2000)) which is a good representative of SST observations. The pattern is symmetric about the equator where it shows a peak with 27°C. Poleward of 60°, the SST is set to 0°C. Between the equator and 60° there

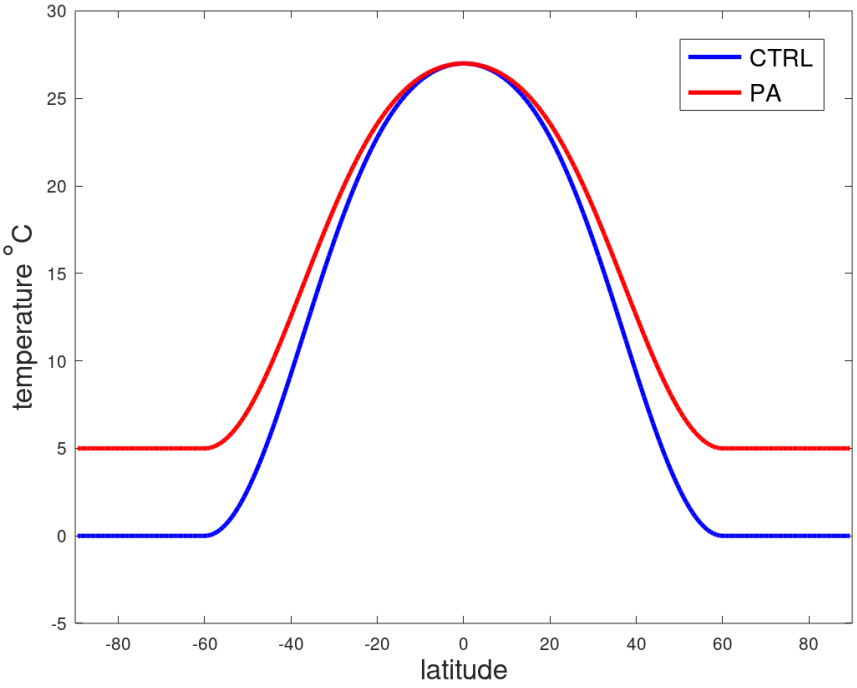

Figure 3.1: Zonal mean SST pattern of the control (CTRL) simulation (blue curve) and the polar amplification (PA) simulation (red curve). The equations describing the SST distribution can be found in Appendix B.

is gradual decrease in the SST. The CTRL SST distribution is revealed by Fig. 3.1 (blue curve). The atmospheric state was initialized from a randomly selected re-analysis (provided by ECMWF). At first, the re-analysis was modified by changing the surface mask to ocean cover and setting the geopotential to zero everywhere at the surface. Finally, the atmospheric fields were interpolated to the new flat surface in those regions where topography was removed. Note that the set-up for the CTRL simulation is identical as in Sinclair et al. (2020).

3.2.2 Polar amplification (PA) simulation

In the polar amplification experiment the ocean surface became warmer almost everywhere (Fig. 3.1, red curve). Polar areas (60-90°) were warmed uniformly by 5°C. Temperature increase in midlatitudes and in the subtropics were smaller,

for example at 40° the temperature increase was 3.33°C. In this experiment the average global temperature increase is 3.1°C with 5°C polar amplification which resembles mostly with CMIP5 multi-model surface temperature outputs between 2081-2100 under RCP 6.0 emission scenario according to Collins et al. (2013). The SST gradient has also changed: overall, the SST gradient decreased in every latitude and the maximum SST gradient moved 0.7° equatorward. In other terms, the PA simulation is identical to the CTRL experiment. Note also that the mathematical development of the SST distributions can be found in Appendix B.

3.2.3 Data analysis

Output fields from the model were saved every six hours containing data on a 512 × 256 grid on 25 pressure levels. For the analysis, atmospheric variables of air temperature, specific humidity, zonal wind, meridional wind and geopotential height was used. As it was mentioned earlier, the analysis covered 5 years of simulation data from the CTRL and from the PA experiment. The data analysis followed the subsequent procedure:

1. Calculating zonal climatology of atmospheric variables:
    - Create zonal and time mean fields of temperature, zonal wind, meridional wind, specific humidity and geopotential height by applying Eq. 2.2 and Eq. 2.4
    - Generate fields of zonal and time mean mass stream function from the zonal and time mean meridional wind field by applying Eq. 2.10
2. Decomposing atmospheric circulation into 3 components following the work of Oort and Peixóto (1983):
    - Gain meteorological fields of mean meridional circulation, stationary eddies and transient eddies

- By using Eq. 2.6 for individual variables and Eq. 2.9 for the product of two variables (e.g. temperature and meridional wind)
- The time averaging period in Eq. 2.6 and Eq. 2.9 was set to 1 month
- 1 month is an appropriate choice, since it is approximately the upper limit for the timescale of transient eddies

3. Obtaining meridional energy transport in different forms of energy:

   - Potential energy (Eq. 2.14), sensible heat/atmospheric enthalpy (Eq. 2.17), latent heat (Eq. 2.15) and kinetic energy (Eq. 2.16) transport was calculated by combining the energy equations with the meridional (v) wind
   - The energy transport was decomposed into the 3 circulation components (see the highlighted term from the integral in Eq. 2.18)
   - Finally, the meridional energy transport was vertically integrated and calculated for a latitude circle by using Eq. 2.18

4. Results

This chapter focuses on the response of atmospheric general circulation to polar amplification on an aqua planet based on the numerical model experiments described in section 3.2 and attempts to address the aims of this paper written at the end of Chapter 1.

4.1 Observed mean state of the atmosphere and changes by polar amplification

This section addresses aim 1 "to quantify how the zonal and time mean temperature, zonal wind, meridional wind, specific humidity and mass stream function reacts to polar amplification on an aqua planet". Note, that time mean here equals with 5-year average.

4.1.1 Zonal mean temperature response

The vertical cross section of the zonal and time mean temperature field of the CTRL simulation (Fig. 4.1) resembles long-term atmospheric observations shown in Fig. 2.1, however, the temperature field is more symmetric about the equator on an aqua planet due to the absence of continents. The temperature response of polar warming is revealed by Fig. 4.2. which shows the temperature difference between the PA and CTRL simulations. Based on Fig. 4.2 we detected intense

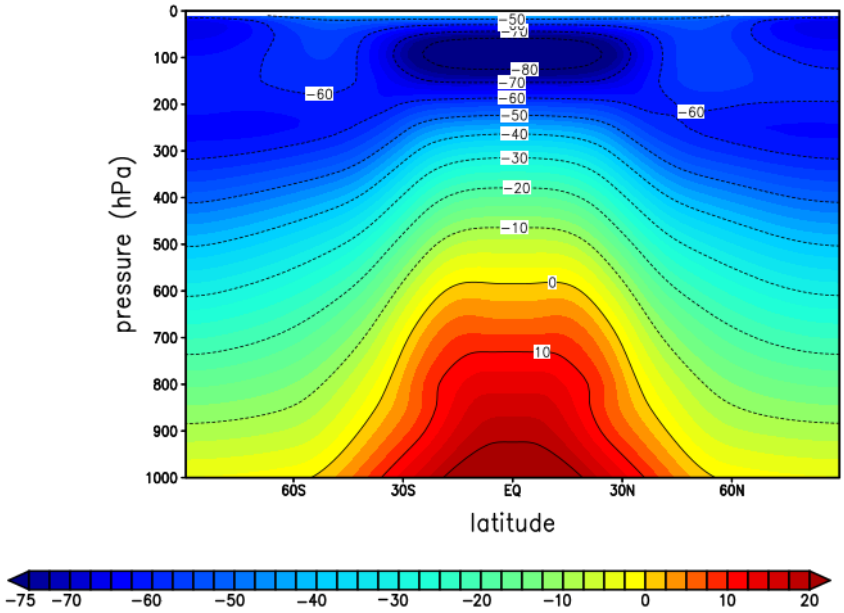

Figure 4.1: Vertical cross-section of the zonal and time mean temperature (°C) of the CTRL aqua planet simulation.

warming of the troposphere over midlatitude and polar areas especially in lower and middle levels (i.e. between 1000 and 700 hPa). The magnitude of lower tropospheric warming exceeds 4.5°C in high latitudes (i.e. 60-90°). Moderate warming (0.5-2°C) is present in the lower troposphere of subtropical areas. Equatorial areas show cooling throughout the whole troposphere and the magnitude of cooling increases with elevation. In the stratosphere, the temperature response is reversed, since there is warming over tropical regions and cooling in higher latitudes. Table 4.1 shows the mean changes of meridional temperature difference between the equator and 60° in various levels. It can be deduced that the meridional temperature difference decreases in case of PA experiment in the troposphere. We also observed that the temperature difference between 0 and 60° is the strongest in the mid-troposphere. Although it is not the central part of this thesis, we note that in the stratosphere we observed slight increase in meridional temperature difference. We also analysed the vertical and zonal mean day-to-day variability of the temperature (revealed by Fig.

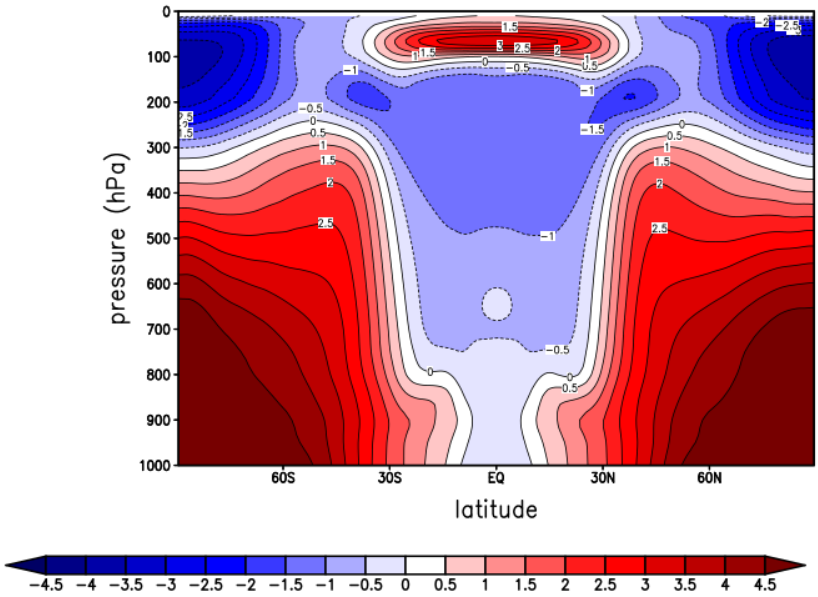

Figure 4.2: Vertical cross-section of the difference in zonal and time mean temperature (°C) between PA and CTRL aqua planet simulations.

10.1 of Appendix C) which also decreases sharply by polar warming in all latitudes, especially in midlatitude areas (up to -28%), which could induce reduction in heat transport by transient eddies.

Table 4.1: Average temperature difference between 0° and 60° (regarding both hemispheres) in various pressure levels in the CTRL and in the PA experiment.

	CTRL experiment	**PA experiment**
850 hPa	26.25°C	21.15°C
500 hPa	29°C	25.5°C
250 hPa	17.5°C	16.5°C
25 hPa	1.3°C	2.5°C

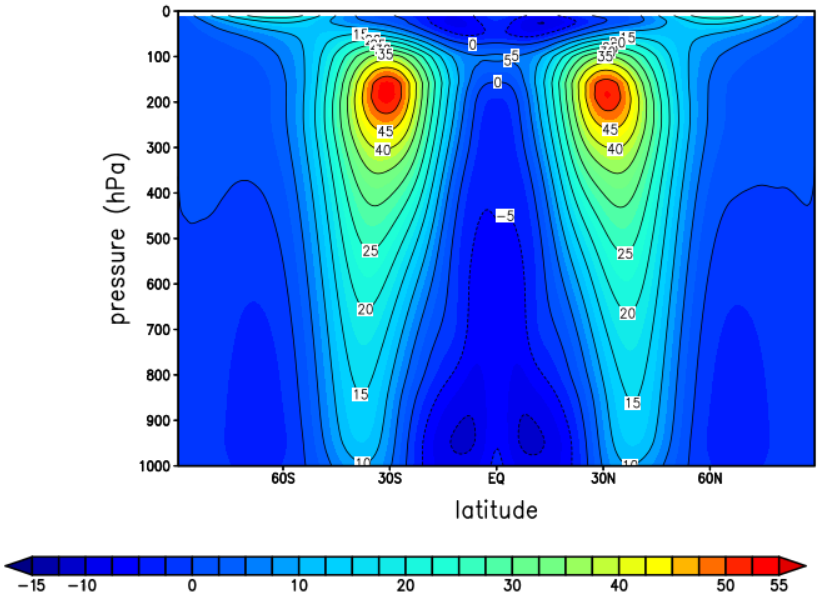

Figure 4.3: Vertical cross-section of the zonal and time mean u-wind ($m\ s^{-1}$) of the CTRL aqua planet simulation.

4.1.2 Zonal mean zonal wind response

The zonal and time mean zonal wind field of the CTRL aqua planet simulation is shown by Fig. 4.3. The zonal wind pattern is similar to long-term observations (Fig. 2.2). On the aqua planet there are surface easterlies in the tropics and surface westerlies in midlatitude areas. In addition, the wind maxima are found in the region of the subtropical jet stream in 35° at 200 hPa. The main difference is in the magnitude of the subtropical jet stream which is 10-15 $m\ s^{-1}$ higher on the aqua planet. By polar amplification the strength of the subtropical jet stream reduces substantially (by approximately 10 $m\ s^{-1}$) which can be explained partly by the reduction of the lower-tropospheric meridional temperature gradient (i.e. thermal wind law, Eq. 2.1) and partly by conservation of angular momentum (for details see Section 4.1.3). It is also observed that the core of the subtropical jet stream shifts 2-2.5 degrees equatorward. The differences between the PA and CTRL simulation is presented by Fig. 4.4 which also shows that surface winds reduce on

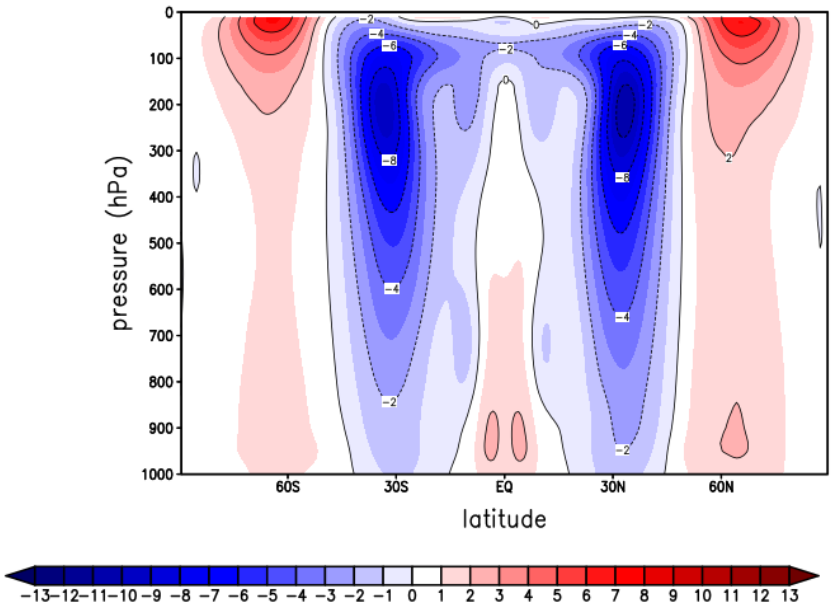

Figure 4.4: Vertical cross-section of the difference in zonal and time mean u-wind ($m\ s^{-1}$) between PA and CTRL aqua planet simulations.

the whole planet including easterly zonal winds, which get less negative and this change is visualised as positive difference on Fig. 4.4. Regarding the stratosphere wind velocities increase in high latitudes which is a result of the increased meridional temperature gradient revealed by Table 4.1. The vertical and zonal mean day-to-day variability of zonal wind (Figure 10.2 of Appendix C) shows a similar pattern as the temperature variability (Fig. 10.1) which possibly causes reduced eddy kinetic energy content.

4.1.3 Response of the mean meridional circulation

As it was presented in Section 2.1.3, the mean meridional circulation can be described by the mass stream function which gives the northward mass transport above a specific pressure level. The stream function of the CTRL and the PA aqua planet simulation is shown by Fig. 4.5. On the aqua planet the Hadley and the Ferrel cells are clearly distinguishable which are more or less symmetric about the

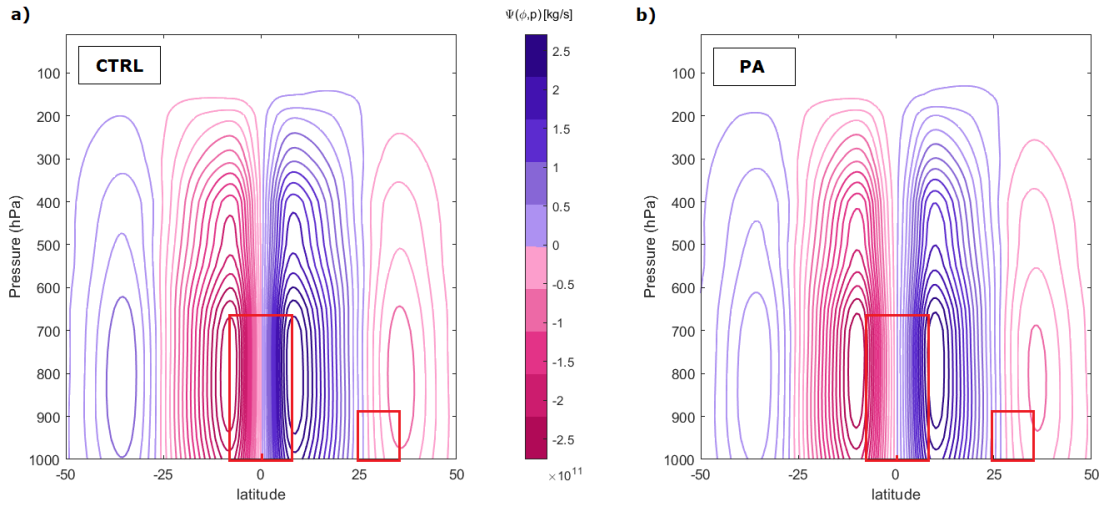

Figure 4.5: Vertical cross-section of the zonal mean mass stream function expressed in $kg\ s^{-1}$. Panel a) shows the results of the CTRL aqua planet simulation and panel b) shows the results of the PA aqua planet simulation. The red boxes are intended to help in identifying the major changes in between the two simulations.

equator. The mass transport of the polar cell is very small and does not appear on the figure. The outcome of the PA simulation reveals that major changes occur in the Hadley cell: mass transport at the equator weakens by 25-30%, the location of maximum transport also weakens (up to -20%) and it shifts 2 degrees poleward. The weakening of the Hadley cell may decrease northward angular momentum transport which in turn weakens the subtropical jet stream. The poleward shift of the maximum transport of the Hadley cell relocates the rising branch of the cell. This causes inter alia less intense lifting of air at the equator, thereby decreasing the atmospheric moisture content in equatorial areas (shown in Section 4.1.4). Furthermore, by polar amplification the Ferrel circulation also reduces approximately by 10% and the location of the maximum transport also shifts 2 degrees poleward. The slowdown of the mean meridional circulation observed in PA simulation induces decreased energy transport by this transport mode.

The mean meridional circulation can be further described by the zonal mean meridional component of the wind (i.e. v-wind) which is represented by Fig. 11.1

of Appendix D, which presents the outcomes of the CTRL simulation showing the Hadley cell and the Ferrel cell. By polar amplification (Fig. 11.2) a slowdown of the mean meridional wind can be deduced both in the lower and in the upper troposphere in all regimes, which is consistent with the results of the zonal mean mass stream function.

4.1.4 Response of atmospheric specific humidity

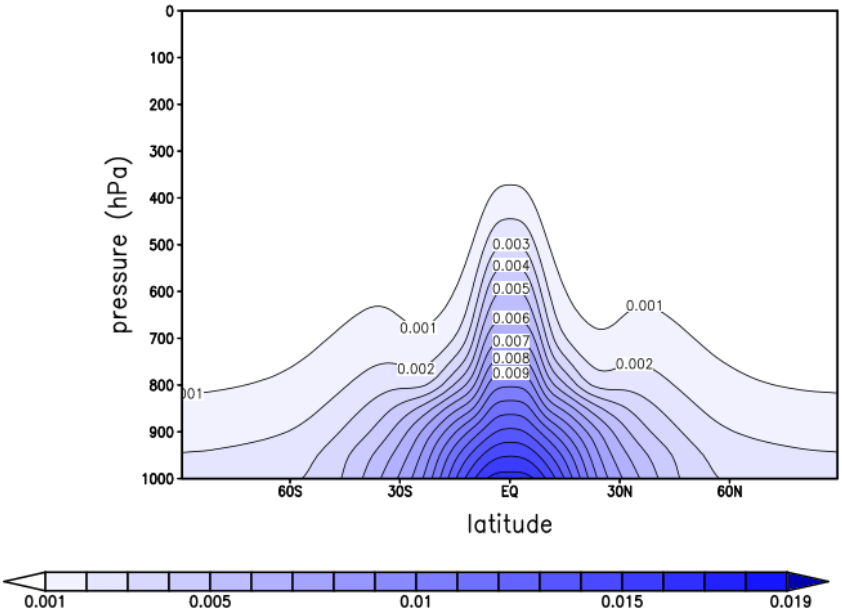

Figure 4.6: Vertical cross-section of the zonal and time mean specific humidity ($kg\ kg^{-1}$) of the CTRL aqua planet simulation.

The specific humidity of the atmosphere of the CTRL aqua planet simulation is shown by Fig. 4.6. It can be seen from the figure that equatorial areas have the largest moisture content, since they are warmer than areas of higher latitudes. The figure also shows a secondary maximum in the middle troposphere in midlatitude areas which is caused by baroclinic eddies. It can be also noticed that the atmospheric moisture content gradually decreases towards the poles. The changes in specific humidity between the PA and CTRL simulation is shown by Fig. 4.7.

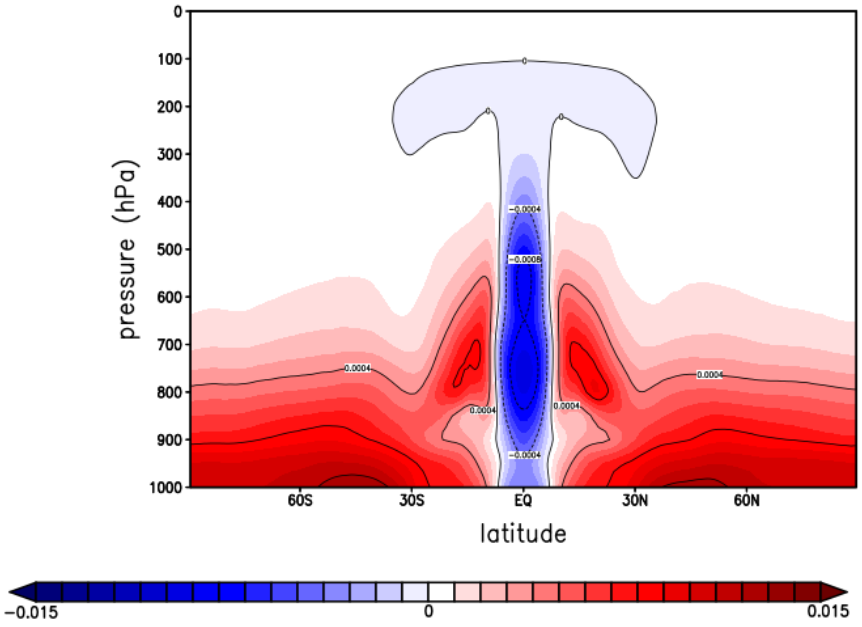

Figure 4.7: Difference in zonal and time mean specific humidity ($kg\ kg^{-1}$) between PA and CTRL aqua planet simulations.

By polar warming, the moisture content of the atmosphere decreases in equatorial areas (between -7 and 7°) and increases in higher latitudes. The largest increase is observed between 30 and 60° in the lower parts of the troposphere (approximately 35% increase between 1000 and 500 hPa). The sharp increase in moisture content of the atmosphere can be explained by atmospheric warming (i.e. a warmer atmosphere can hold more moisture according to the Clausius-Clapeyron equation). In equatorial areas the largest reduction occurs between 850 and 800 hPa. There is also a significant increase in specific humidity at the same level between 10 and 18°. These modifications are explained by the changes occurring in the Hadley cell (shown in the previous section) in which the peak region of the mass transport is shifted 2 degrees poleward by polar amplification. The shifted rising branch of the Hadley cell, which is responsible for moistening middle and upper levels causes lower moisture content in equatorial areas and larger moisture content a few degrees poleward in the middle troposphere. Regarding the meridional moisture gradient at 900 hPa, we observed that it decreases by approximately 10% between 0° and 90° N/S.

However, we also noticed that the decrease is strongest between 0° and 50°, and it is minor between 50° and 90°. The decreased meridional moisture gradient entails decreased meridional moisture flux.

4.2 Meridional energy transport

This section focuses on aim 2 "to inspect how atmospheric meridional energy transport reacts to polar amplification on an aqua planet by **i)** quantifying the zonal and time mean vertical integrals of meridional energy transport of total atmospheric energy, sensible heat, latent energy, potential energy and kinetic energy and by **ii)** quantifying the contribution of mean meridional circulation, transient eddies and stationary eddies to zonal and time mean vertical integrals of meridional total atmospheric energy transport, sensible heat transport, latent energy transport, potential energy transport and kinetic energy transport". Firstly, changes of the total meridional energy transport are presented which is followed by discussing the changes of the different energy forms (i.e. energy forms presented earlier in Section 2.2.1).

4.2.1 Transport of total atmospheric energy

Vertically integrated meridional total energy transport (i.e. including all energy forms) by the CTRL and the PA simulation is shown by Fig. 4.8. The vertically integrated meridional total energy transport of the CTRL simulation (i.e. without decomposing the atmospheric circulation, solid black line) is symmetric about the equator and has a primary peak in the region of the Hadley cell and a secondary peak in the region of midlatitude eddies. These results are comparable with ERA-Interim re-analysis products between 1989 and 2009 (Mayer and Haimberger, 2012). However, in our CTRL aqua planet simulation there is positive difference in

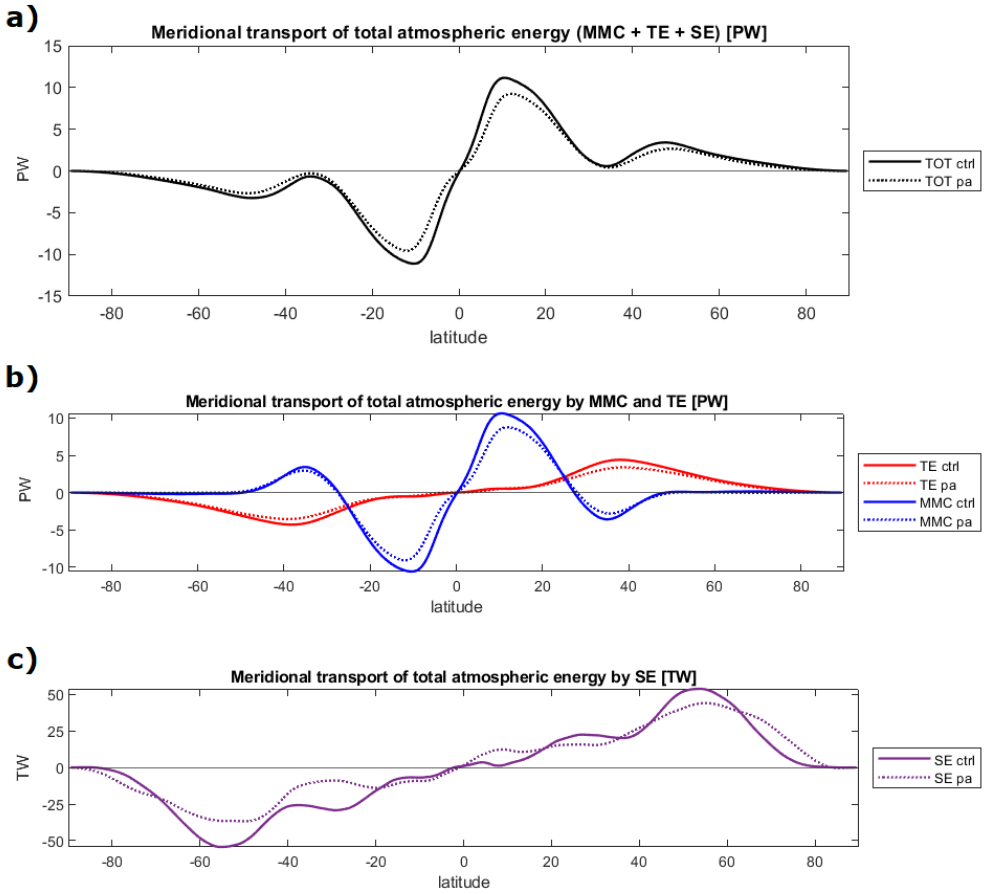

Figure 4.8: Vertically integrated zonal and time mean meridional total atmospheric energy transport composed of flux of sensible heat, latent heat, potential energy and kinetic energy of the CTRL (solid line) and of the PA simulation (dashed line). Positive values mean northward energy transport. Panel a) includes meridional total energy transport composed of the summed transport of mean meridional circulation, transient eddies and stationary eddies in PW ($10^{15} kg\ m^2\ s^{-3}$). Panel b) shows the meridional total energy transport by the mean meridional circulation (blue line) and by transient eddies (red line) in PW ($10^{15} kg\ m^2\ s^{-3}$). Panel c) gives information about the meridional total energy transport by stationary eddies in TW ($10^{12} kg\ m^2\ s^{-3}$).

maximum total meridional atmospheric energy transport (+81%) throughout both hemispheres, and the primary peak in tropical areas does not appear in the reanalysis.

It can be deduced, that vertically integrated meridional total atmospheric energy transport decreases by polar amplification nearly by 15% in 11°N and 21% in

47° on average. Decrease in polar regions is negligible. The changes by MMC and transient eddies are revealed by panel b) of Fig. 4.8. In case of the MMC, the meridional energy flux decreases by polar warming: the Hadley cell transports less energy poleward and the Ferrel cell shows also reduced equatorward energy transport. In case of midlatitude transient eddies, it can be noticed that they transport less energy poleward (-23%), which is partly offset by the meridional energy flux changes in the Ferrel cell. We also observed that the maximum of transient eddy meridional energy flux shifts 0.75° poleward. However, this shift equals only one grid cell of the model, which questions the significancy of this result. It is also important to mention that meridional total energy transport by the MMC and transient eddies are of similar scales. Vertically integrated stationary eddy meridional total energy flux is also visualised on panel c) of Fig. 4.8 whose strength is three orders of magnitude smaller than MMC and transient eddies. In addition, the stationary eddy signal appears to be noisy and it does not show any significant reaction to the PA simulation, therefore the further analysis of stationary eddies is omitted, and we declare that they are not present on an aqua planet on monthly time scale.

4.2.2 Transport of sensible heat

Vertically integrated meridional sensible heat or atmospheric enthalpy transport in the aqua planet simulations is presented by Fig. 4.9. The vertically integrated meridional total atmospheric sensible heat transport ($C_p \left[\overline{vT} \right]$) in the CTRL simulation (black curve) is equatorward in tropical areas (effect of Hadley circulation) and it is poleward in higher latitudes (effect of midlatitude eddies). Vertically integrated meridional sensible heat transport by the MMC ($C_p \left[\bar{v}\right] \left[\bar{T}\right]$; blue curve) equals with total heat transport in tropical areas (i.e. the total transport corresponds to the transport by the Hadley cell in the tropics). In midlatitude areas poleward sensible heat transport by transient eddies ($C_p \left[\overline{v'T'}\right]$) exceeds the poleward heat transport

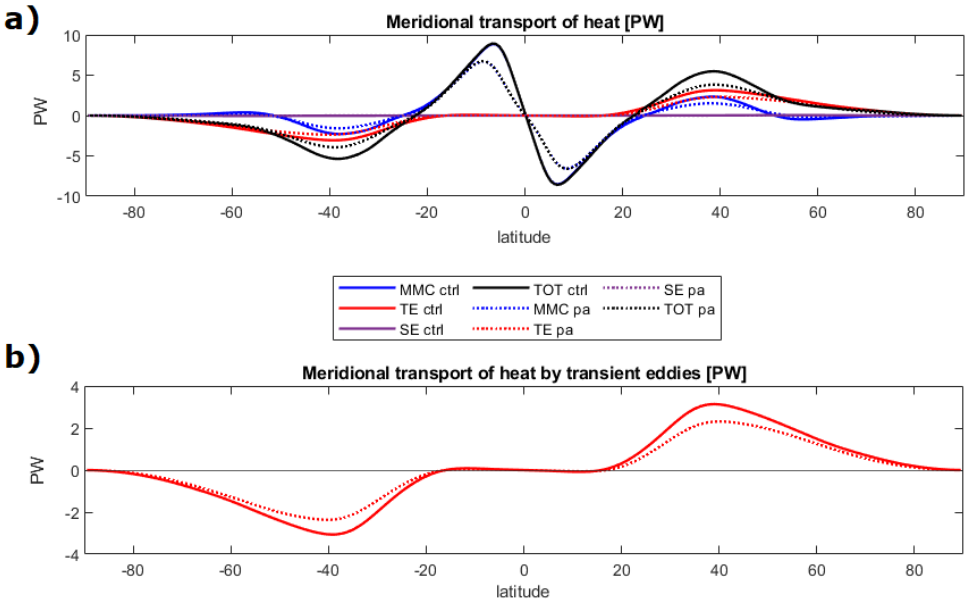

Figure 4.9: Vertically integrated zonal and time mean meridional sensible heat transport of the CTRL (solid line) and of the PA simulation (dashed line) in PW ($10^{15} kg\ m^2\ s^{-3}$). Positive values mean northward energy transport. Panel a) gives information about the meridional total sensible heat transport by all transport modes (black line), the meridional sensible heat transport by the mean meridional circulation (blue line), the meridional sensible heat transport by transient eddies (red line) and the meridional sensible heat transport by stationary eddies (purple line). Panel b) shows only the meridional sensible heat transport by transient eddies.

of the Ferrel cell. The effect of stationary eddies is negligible. It is important to note that these results are highly consistent (in magnitude and in the direction of heat transport) with observations (Fig. 13.6 from Peixoto and Oort (1992)).

The polar amplification experiment indicates reduced meridional sensible heat transport both by MMC and by transient eddies. The average reduction is nearly 23% in case of the Hadley cell, 36% in case of the Ferrel cell and 26% in case of transient eddies. The reduction in vertically integrated sensible heat transport is consistent with the observed slowdown of the mean meridional circulation (Section 4.1.3), and the decrease of the lower tropospheric meridional temperature gradient (Section 4.1.1). Moreover, the reduction of the meridonal transient eddy sensible

heat flux is also in agreement with the reduced standard deviation of time mean temperature (Fig. 10.1).

4.2.3 Transport of latent heat

Atmospheric meridional latent energy transport in the CTRL aqua planet simulation is concentrated in the lower parts of troposphere (i.e. similar to normal atmospheric conditions) and the vertically integrated meridional fluxes are displayed by Fig. 4.10 (solid curves). Vertically integrated meridional total latent energy transport of the

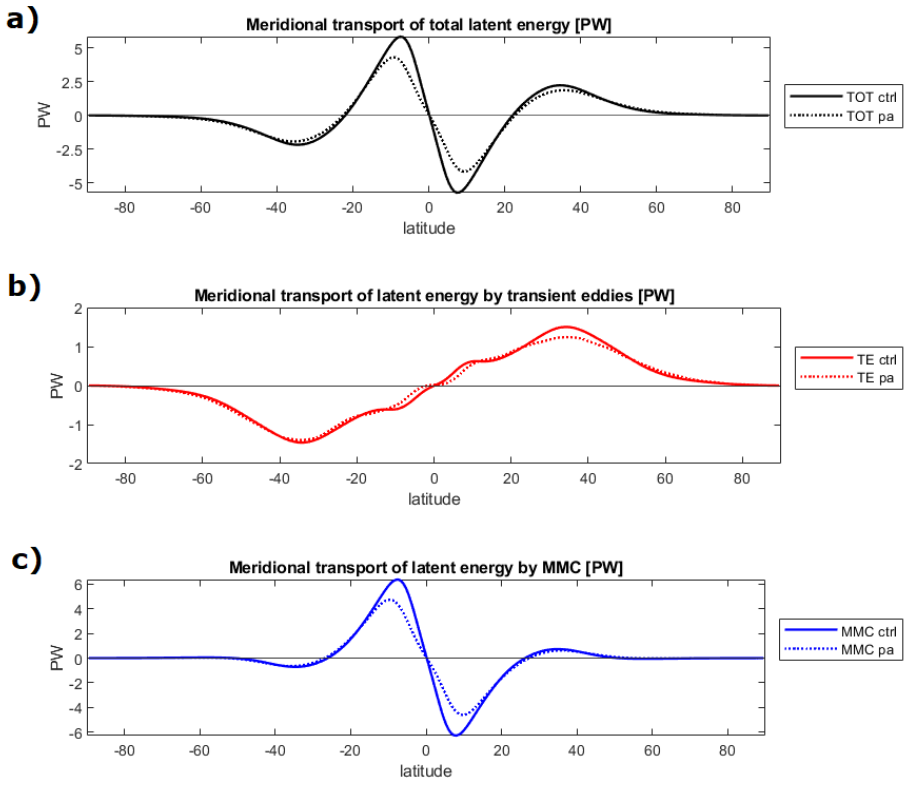

Figure 4.10: Vertically integrated zonal and time mean meridional latent heat transport of the CTRL (continuous line) and of the PA simulation (dashed line). Positive values mean northward energy transport. Panel a) gives information about the meridional total latent heat transport by all transport modes (black line). Panel b) shows only the meridional latent heat transport by transient eddies. Panel c) gives information about the meridional latent heat transport by the MMC. The unit of energy transport is PW ($10^{15} kg\ m^2\ s^{-3}$).

CTRL simulation ($L\,[\,\overline{vq}\,]$; black solid curve) is equatorward in the tropics (effect of Hadley cell) and it is poleward in higher latitudes (combined effect of the Ferrel cell and transient eddies). Vertically integrated meridional latent heat transport by the MMC ($L\,[\bar{v}]\,[\bar{q}]$; blue solid curve) is exceptionally strong in the Hadley cell due to large moisture availability. In case of the Ferrel cell the meridional latent energy flux is 88% less than the transport of the Hadley cell. In case of transient eddies ($L\left[\overline{v'q'}\right]$; red solid curve) the vertically integrated meridional latent heat transport peaks in 34° and it decreases gradually towards the poles. Stationary eddies are negligible in this case as well. The above mentioned results of the CTRL simulation are consistent with observations made by (Oort and Peixóto, 1983) including inter alia the the location of peak meridional latent energy transport by the MMC and transient eddies.

The changes in vertically integrated meridional latent heat flux in the PA simulation is given by the dashed curves of Fig. 4.10. By polar amplification, our experiments show large reduction in vertically integrated meridional latent energy transport in the Hadley cell (up to 27%), whereas the Ferrel cell does show more moderate reduction (nearly 14%). Additionally, in case of the Hadley cell the maximum of meridional latent energy transport moves 1.4° poleward. The changes in the Hadley cell are consistent with the previously observed slowdown and poleward shift of the mean meridional mass transport (Section 4.1.3). Even though midlatitude and polar atmosphere contains more moisture caused by polar warming, the vertically integrated meridional total latent energy transport does not increase in these areas remarkably, in fact transient eddy meridional latent heat flux slightly decreases between 23 and 51°. In latitudes higher than 51° there is slight positive change in meridional latent energy transport by transient eddies which peaks at 61° with a change of +0.065 PW (+28%). We note that this result is consistent with the changes of meridional moisture gradient described in Section 4.1.4.

Overall, we came to the conclusion that higher moisture availability in higher latitudes and the slight change of meridional moisture gradient 50-90° counteracts the effect of slowdown of atmospheric circulation due to polar amplification, however, this counter-effect is not enough to substantially increase the atmospheric meridional total energy flux.

4.2.4 Transport of potential energy

Vertically integrated meridional potential energy transport in the CTRL aqua planet simulation can be followed by the solid curves of Fig. 4.11. As it was expected, most of the meridional potential energy flux comes from the mean meridional circulation ($g\left[\bar{v}\right]\left[\bar{Z}\right]$; blue continuous curve) which is towards the poles in the region of the Hadley cell and it is equatorward within the Ferrel cell. In the Hadley cell the meridional potential energy transport (24.3 PW) exceeds the magnitude of the sum of latent and sensible heat transport (-14.8 PW), which causes overall poleward

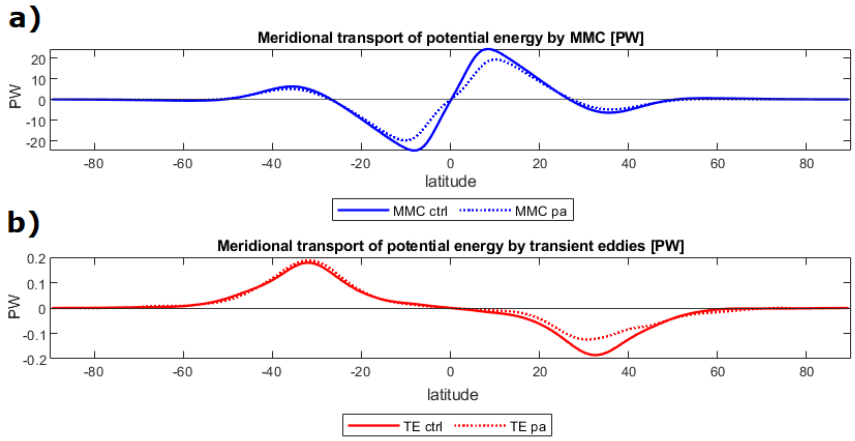

Figure 4.11: Vertically integrated zonal and time mean meridional potential energy transport of the CTRL (continuous line) and of the PA simulation (dashed line). Positive values mean northward energy transport. Panel a) shows the meridional potential energy transport by the mean meridional circulation. Panel b) gives information about the meridional potential energy transport by transient eddies. All values are expressed in PW ($10^{15} kg\ m^2\ s^{-3}$).

energy transport (consistent with long-term observations described in Section 2.2.2). In the Ferrel cell, the magnitude of vertically integrated meridional potential energy transport is much less than in the Hadley cell. The vertically integrated potential energy flux by transient eddies ($g\left[\overline{v'Z'}\right]$; red continuous curve in Fig. 4.11) is two orders of magnitude smaller than the MMC peaking in 33° and the direction of energy transport is towards the equator. This is also reasonably consistent with observations (i.e. Fig.13.7b from Peixoto and Oort (1992)).

The polar amplification simulation (dashed lines in Fig. 4.11) shows decreased potential energy transport by the MMC, especially in the Hadley cell, where the decrease is approximately 20.5%. Moreover, we observed poleward shift of the maximum poleward potential energy transport of the Hadley circulation (approximately 1.4°). The flux by transient eddies in the PA simulation (dashed red curve) is not symmetric about the equator and the change is not evident due to the noisiness of the signal. Overall, the meridional potential energy flux decreases by polar warming.

4.2.5 Transport of kinetic energy

Vertically integrated meridional kinetic energy transport of the aqua planet simulations can be followed by Fig. 4.12. Here, we turn a special focus on the convergence of mean kinetic energy in the subtropics, since it is an indicator of the strength of the subtropical jet stream (Section 2.2.2). First, we deal with the results of the CTRL simulation (solid curves). The total meridional kinetic energy transport ($\frac{1}{2}\left[\bar{v}\left(\overline{u^2}+\overline{v^2}\right)\right]$; solid black curve in Fig. 4.12) including all of the energy transport modes determines one convergence centre of kinetic energy at 26° which is associated with the subtropical jet stream. The meridional kinetic energy transport of the mean meridional circulation ($\frac{1}{2}\left[\bar{v}\right]\left([\bar{u}^2]+[\bar{v}^2]\right)$; solid blue curve in Fig. 4.12), contributes most to meridional kinetic energy flux. The MMC transports kinetic energy poleward between 12 and 26° and equatorward between 26° and 50°, and

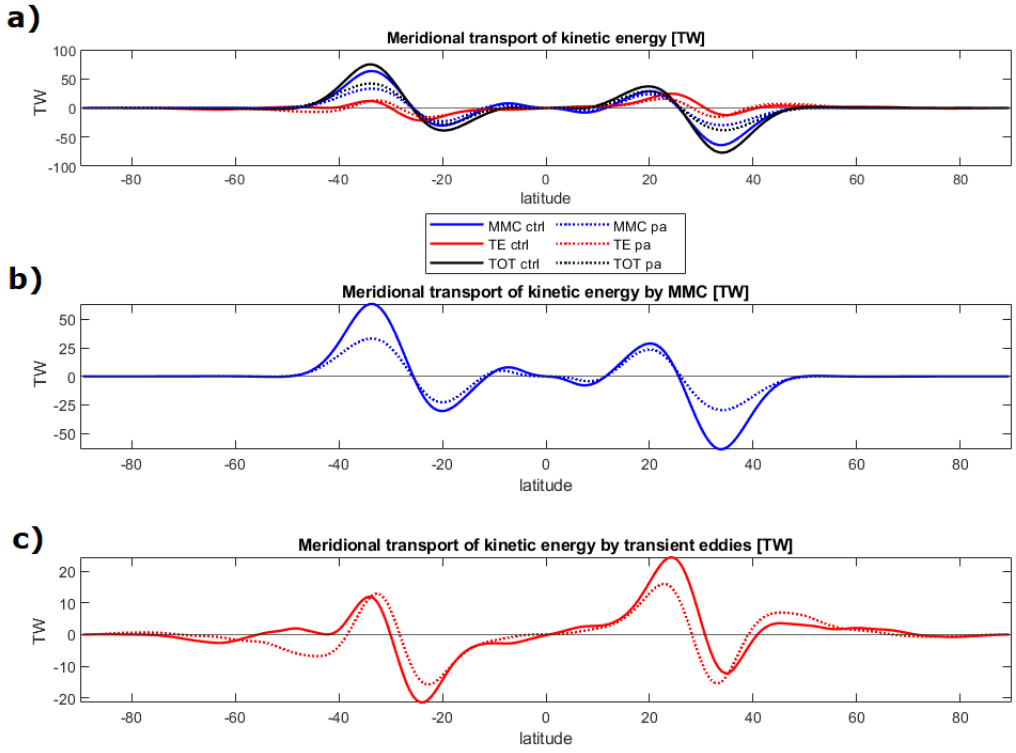

Figure 4.12: Vertically integrated zonal and time mean meridional kinetic energy transport of the CTRL (solid line) and of the PA simulation (dashed line) in TW ($10^{12} kg\ m^2\ s^{-3}$). Positive values mean northward energy transport. Panel a) gives information about the meridional total kinetic energy transport by all transport modes (black line), the meridional kinetic energy transport by the mean meridional circulation (blue line) and the meridional kinetic energy transport by transient eddies (red line). Panel b) represents meridional kinetic energy flux by the mean meridional circulation. Panel c) shows the meridional transient eddy kinetic energy flux.

this causes convergence of vertically integrated kinetic energy at the location of the subtropical jet stream. Vertically integrated meridional kinetic energy transport by transient eddies ($\frac{1}{2}\left[\overline{v'\left(u'^2+v'^2\right)}\right]$;solid red curve in Fig. 4.12) slightly differs from equatorial symmetry and it has also a well-defined convergence center at 31°, which can be associated with the eddy-driven jet. The meridional kinetic energy transport in the CTRL simulation differs from observations in two senses:

- the transient eddy component is lower than the MMC component in the CTRL simulation, however observations show that the transient eddy component

ought to exceed the MMC component (Oort and Peixóto, 1983);

- there should be a convergence center of transient eddy kinetic energy at 55° (Oort and Peixóto, 1983), more poleward compared to our simulations (i.e. 31°).

The polar amplification simulation (dashed curves on Fig. 4.12) shows reduced total and mean meridional kinetic energy transport leading to lessening convergence of kinetic energy at 26° which is consistent with the weakening of the subtropical jet stream described in Section 4.1.2. The transport by transient eddies shows some modifications which are ambiguous (red dashed curve in Fig. 4.12). We observed equatorward shift of the convergence center of vertically integrated transient eddy meridional kinetic energy transport at 31°, which can indicate equatorward shift of the eddy-driven jet. Changes of kinetic energy flux by transient eddies in midlatitude and polar areas is contradictory. The results indicate increase of transient eddy poleward kinetic energy transport even though we observed decreased transient eddy kinetic energy content and previous results suggest weakened transient eddies. However, explaining these caveats is not part of this thesis and we recommend further research concentrating on this specific problem.

Rgearding the kinetic energy content of the atmosphere, we noticed that it occurs mainly in the upper troposphere. The mean component of kinetic energy ($\frac{1}{2}\left([\bar{u}^2] + [\bar{v}^2]\right)$; Fig. 12.1 in Appendix E) is concentrated at the location of the subtropical jet stream (around 30° at 200 hPa). The transient eddy component of kinetic energy ($\frac{1}{2}\left[\overline{u'^2} + \overline{v'^2}\right]$; Fig. 13.1 in Appendix F) can be found in the upper troposphere (between 200 and 300 hPa) in 35-50°. By polar amplification the kinetic energy content of the atmosphere decreases notably, the maximum reduction of the mean component (Appendix E, Fig. 12.2) is more than 30% and the maximum reduction of the transient eddy component (Appendix F, Fig. 13.2) reaches 27%.

5. Discussion

In this chapter we interpret and compare our results (presented in Chapter 4) with similar studies.

5.1 Observed mean state of the atmosphere

Previously, it was described how the zonal mean temperature, horizontal wind, specific humidity and mass stream function reacted to polar amplification on an aqua planet (Section 4.1). Comparing the temperature response to ensemble CMIP5 GCM projections for the end of the 21st century under the RCP 8.5 emission scenario, we can deduce some similarities with our findings. In general, CMIP5 GCM future projections predict enhanced warming in the tropics in the higher troposphere and they also show surface polar amplification which extends to the mid-troposphere (Vallis et al., 2015; Feldl et al., 2017; Yuval and Kaspi, 2020). Our PA simulation forced by SST also shows increased lower and middle tropospheric warming in higher latitudes, but the tropical upper tropospheric warming does not appear, in fact we detected slight cooling in the equatorial tropospheric column. In addition, we also observed reduced meridional temperature gradient throughout the troposphere.

An early, but rather important global warming model study by Manabe and Wetherald (1980) showed intense polar amplification under $2 \times CO_2$ (600 ppm CO_2) and $4 \times CO_2$ (1200 ppm CO_2) experiments. In this study, they performed idealized GCM simulations without seasonal cycle of insolation, with idealized geography free

of mountains and with a snow cover scheme. In the $2 \times CO_2$ experiment they found that polar amplification extends to the lower and middle troposphere and towards midlatitude areas as well, similar to the results presented in this thesis. They also found reduced meridional temperature gradient in the lower troposphere.

In our PA simulation the subtropical jet stream showed reduced strength as a response to decreased low-level meridional temperature gradient and reduced intensity of the Hadley cell. The reduced convergence of mean kinetic energy at 26° is also consistent with the weakening of the subtropical jet stream. Similar zonal wind response appears also in the results of Manabe and Wetherald (1980) and in Yuval and Kaspi (2020). The latter study utilized idealized GCM simulations with a Newtonian cooling scheme to produce desired zonal mean temperature distributions. This scheme allowed the authors to investigate how different spatial structures of temperature modify atmospheric circulation. Inter alia, they investigated different temperature patterns of polar amplification and they also found reduced zonal winds at the location of the subtropical jet stream.

In the experiments presented here, atmospheric moisture content increased almost everywhere. This is in agreement with simulations presented by Manabe and Wetherald (1980) and Feldl et al. (2017). The latter study used the GFDL AM2.1 GCM in its aqua planet configuration with seasonally varying insolation under quadrupling of CO_2 including prescribed ice albedo values which enabled them to generate polar amplification with different strength. In addition, Held and Soden (2006) found also enhanced atmospheric moisture content using climate change experiments designed for IPCC 4th Assessment Report.

Regarding the mean meridional circulation response in our experiments, we can declare that it has weakened in the Hadley cell and in the Ferrel cell. In addition, the maximum mass transport in the Hadley cell shifted 2 degrees poleward based on the response of zonal mean stream function. Comprehensive GCM model experiments

of CMIP5 simulating future climate agree on that the Hadley cell weakens and expands poleward in response to tropospheric warming caused by radiative forcing (Vallis et al., 2015; Hu et al., 2018). The projected weakening of the MMC can be interpreted by thermodynamic processes according to Held and Soden (2006) and Vallis et al. (2015). Based on the work of Held and Soden (2006), global precipitation does increase with warming, but not as steeply as atmospheric moisture content. This in turn suggests that the exchange of mass between the boundary layer and the mid-troposphere may decrease. This could reduce atmospheric circulation, particularly in the tropics where the role of vertical moisture transport by Cumulus convection is enhanced (Held and Soden, 2006). This mechanism can be supported by our aqua planet experiments, since we found increase of atmospheric moisture content poleward of 11°, and 20% reduction of the maximum mass transport in the Hadley cell. Other theoretical explanations for the weakening of the Hadley cell due to global warming include the effect of subtropical static stability and eddy momentum flux divergence (Vallis et al., 2015) which are not discussed in this thesis.

In addition, Levine and Schneider (2011) investigated the response of the Hadley circulation to future warming/cooling in an idealized GCM in its aqua planet configuration coupled to a simple representation of ocean heat transport. Likewise in this thesis, they used the zonal mean mass stream function to describe the mean meridional circulation which makes our results more comparable. They found that as climate warms the Hadley cell weakens which is consistent with our findings. In their paper they also investigated the location of the subtropical jet stream, and they found that it moves 0.26°/K poleward relative to global surface temperature increase. In our experiments, the subtropical jet stream shifted 2-2.5 degrees equatorward, which is not consistent with their results. However, we note that the location of the maximum SST gradient in the PA experiment moved 0.7 degrees equatorward which may explain the equatorward shift of the subtropical jet stream.

5.2 Meridional energy transport

5.2.1 Total meridional energy transport

We observed markedly reduced atmospheric poleward energy transport due to polar amplification, however, the reduction was not the same for different forms of energy (Section 2.2.1) and for different modes of energy transport (Section 2.2.2). Overall, the vertically integrated zonal mean poleward total energy transport decreased in all regions. The highest decrease occurred in the region of the Hadley cell (-18%) and in the region of midlatitude baroclinic eddies (-24%). Moreover, we have also seen that the dry static energy transport (i.e. the sum of sensible heat and potential energy transport) decreased across the globe. The total latent energy transport also showed reduction between 0 and 51° and no remarkable change was found further poleward.

Caballero and Langen (2005) also analysed the changes of meridional energy transport by polar amplification through a set of idealized aqua planet model simulations by an atmospheric model of NCAR (namely, PCCM3). Their aim was to investigate the relationship between poleward energy transport, global mean surface temperature (T_m) and meridional temperature gradient at the surface (ΔT). Their model configuration was slightly different than ours, since it allowed the SST to be below 0°C and the model included a sea ice scheme. They calculated the meridional energy transport in a different way compared to our method: they derived the energy flux indirectly by calculating the difference between time mean vertically integrated energy flux at model top and at surface. They found that extratropical peak meridional atmospheric energy transport increases with T_m and with ΔT. Their results (represented by Fig. 5.1) are highly comparable to our findings. Our CTRL experiment having a mean SST of 10.15°C (T_m) and a pole-to-Equator temperature gradient of 27°C (ΔT) with peak extratropical total meridional energy transport of

3.41 PW in 47° is fairly close to the value (around 3 PW) that could be predicted by their findings (see Fig. 5.1). The difference based on this is only 0.3-0.4 PW. The PA experiment (with T_m=13.27°C and ΔT=22°C) shows peak extratropical total meridional energy transport (2.66 PW) in 49°, which is also close to the findings (around 2.4 PW) of Caballero and Langen (2005) having a difference of only 0.2-0.3 PW.

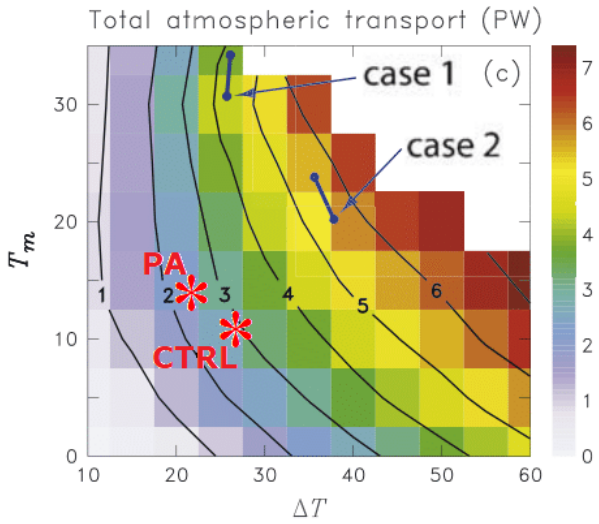

Figure 5.1: Peak extratropical poleward transport of total energy as a function of surface meridional temperature gradient (ΔT) and global mean surface temperature (T_m) acoording ot Caballero and Langen (2005). Red segments represent our CTRL and PA aqua planet simulation discussed in Section 3.2. The blue segments represent slab ocean simulations carried out by Caballero and Langen (2005) (not discussed in this thesis). Figure adopted from Caballero and Langen (2005).

Research by Hwang et al. (2011) also concentrated on couplings between polar amplification and poleward energy transport. They used 20 different CMIP3 GCM simulations under A1B and A2 scenario to study the changes of poleward energy transport between 2081-2100 and 2001-2020. All simulations predicted increased lower-tropospheric moisture content with increased poleward moisture transport, however, this was counterbalanced by the decrease of dry static energy transport, which was the dominating energy transport form of the inter-model spread. They

also showed that the degree of polar amplification is negatively correlated with northward energy transport: the higher the polar amplification, the less the increase of poleward energy transport, which can be a decrease if the magnitude of polar amplification is high.

An earlier GCM model study by Colman et al. (1994) investigating the changes of annual mean meridional energy transport under doubling the atmospheric CO_2 content had similar results compared to the previous studies. The authors used the same approach for calculating the meridional energy transport as in this thesis (described in Section 2.2.2). They found decreased pole-to-Equator temperature gradient and reduced total poleward energy transport between 0 and 65°. Another study concentrating partly on polar amplification and atmospheric meridional energy transport on an aqua planet by Feldl et al. (2017) found that by polar amplification the dry static energy flux decreases and latent energy flux increases. However, under strong polar warming the relative importance of latent energy flux to total energy transport reduces, hence the poleward energy flux decreases. Alexeev et al. (2005) also suggests that polar amplification may weaken poleward energy transport when equilibrium is reached even though the transport is increasing in the transient phase of aqua planet GCM simulations.

After all, it is important to mention that some authors observed that polar amplification increases poleward energy transport. For example, Held and Soden (2006) came to the conclusion that meridional total energy transport increases under global warming simulations in AR4 models (i.e. models used for the 4th Assessment Report of the IPCC) and this increased poleward energy transport is dominantly caused by the increased moisture transport. Moreover, O'Gorman and Schneider (2008) simulated wide range of general circulations with an idealized moist GCM to test how the global hydrological cycle and energy transport changes as the climate warms or cools. According to their results, the total meridional energy transport at

50° increases slightly with warming climate, however there is saturation when the global mean surface air temperature reaches $300K$.

5.2.2 Eddy energy transport

Regarding the response of transient eddies, our simulations showed that the total meridional energy transport by transient eddies decreases by polar amplification, which is mainly caused by the decreased meridional sensible heat flux. It was also interesting to see that the meridional latent energy flux by transient eddies decreased between 23 and 51°and did not increase further poleward. This feature is probably due to the changed meridional moisture gradient which decreased between 0 and 50°, and increased slightly poleward of 50°. In contrast, results of Feldl et al. (2017) show that meridional latent heat transport increases with strengthening polar amplification on an aqua planet. However, the surface warming in their study is different than our experiments which may generate differences in meridional moisture gradient. In addition, their study also showed decreased meridional total energy transport by transient eddies, similarly to our findings. Results by Colman et al. (1994) regarding transient eddy meridional energy transport response to doubling CO_2 content of the atmosphere with polar amplification is somewhat different than our findings. In their paper they presented that there is large decrease in transient eddy poleward energy transport between 60°S and 45°N which is dominated by changes in sensible heat transport. In polar areas they found increased transient eddy poleward energy flux which was caused by the increase of latent heat transport.

Results of Yuval and Kaspi (2020) who investigated the atmospheric response to different global temperature patterns (presented earlier in Section 5.1) demonstrates that the eddy heat flux decreases by polar amplification. They also showed that the eddy kinetic energy (EKE) content of the atmosphere also decreases by polar amplification when surface temperature increase is restricted to polar areas.

This is consistent with our findings, since we also showed markedly reduced transient eddy kinetic energy content as a response to polar amplification. In addition, Manabe and Wetherald (1980) also found lessening EKE in the doubling CO_2 simulation in an idealized GCM.

In the CTRL simulation, the transient eddy meridional kinetic energy transport disagrees with observations. The response of the transient eddy meridional kinetic energy to polar warming in midlatitudes and in polar areas is also conflicting and we recommend further research focusing on this issue.

Furthermore, we omitted discussing the stationary eddy response to polar amplification, since we declared earlier that there is no mechanism that would support generation of stationary eddies on an aqua planet. Caballero and Langen (2005) and Feldl et al. (2017) also did not discuss stationary eddies in their aqua planet model studies.

Lastly, we note the most relevant limitations of our experiments. We did not include an ocean model to our simulations, thus we were not considering energy transport by the ocean. In addition, we simulated polar amplification with only one SST profile which also includes surface warming outside of polar areas. We also mention that we used 1 month for the time averaging period during data analysis and this did not resulted in a stationary eddy signal. Changing this period (for example to 15 days) might alter our results, therefore further research is needed.

6. Conclusion

In this thesis we studied how the atmospheric general circulation adjusts to polar amplification on an aqua planet in terms of the response of zonal mean atmospheric state and the response of meridional energy transport. We studied the changes in energy transport by decomposing the general circulation to the mean meridional circulation, transient eddies, and stationary eddies. We studied polar amplification by carrying out numerical model experiments with OpenIFS global NWP model in its aqua planet configuration. The experiments were forced by different SST patterns. For the data analysis, 5 years of data has been used.

We found considerable tropospheric warming in polar and midlatitude areas, and in the subtropical lower troposphere due to polar amplification. In equatorial areas, we found tropospheric cooling. The zonal mean zonal wind response showed reduced intensity of the subtropical jet stream. The mean meridional circulation showed reduced strength and the maximum transport of the Hadley cell shifted 2 degrees poleward relocating the rising branch away from the equator. The reduced lifting in equatorial areas due to the poleward shift of the rising branch of the Hadley cell might explain the observed tropospheric cooling in this region. The slowdown of the mean meridional circulation and the reduced strength of the subtropical jet stream is consistent with the decreased surface and lower-tropospheric meridional temperature gradient. The atmospheric specific humidity content has also increased due to polar amplification, particularly in midlatitude and in polar areas. This result

is physically consistent, since if the atmosphere warms it can hold more moisture.

Regarding the meridional energy transport, we found that the vertically integrated meridional total energy transport decreased in all latitudes. The decrease was relatively high in the region of the Hadley cell and in the region of baroclinic eddies. Reduced vertically integrated meridional energy transport by the mean meridional circulation was present in case of potential energy, sensible heat, latent heat, and kinetic energy. In case of the meridional kinetic energy transport by the mean meridional circulation, we found reduced convergence of mean kinetic energy in 26° which is consistent with the weakening of the subtropical jet stream. Transient eddies also showed reduced poleward total energy transport which was caused by the major decrease in meridional sensible heat transport. Unlike many other studies, we detected that the transient eddy latent heat transport decreased between 23 and 51° and it did not increase marginally poleward of 51° despite the increased moisture content of the atmosphere. The changes in meridional moisture gradient might explain this observation. To add some more, we did not detect stationary eddies in our simulations due to the absence of the primary forcing mechanisms.

As a final conclusion, we have seen that polar amplification causes major changes in atmospheric general circulation on an aqua planet. Our results suggest that atmospheric meridional energy transport loses strength and overall, less energy is transported towards the poles by the atmosphere.

Bibliography

Alexeev, V., Langen, P. and Bates, J. (2005), 'Polar amplification of surface warming on an aquaplanet in "ghost forcing" experiments without sea ice feedbacks', *Climate Dynamics* **24**(7-8), 655–666.

Bintanja, R., Van der Linden, E. and Hazeleger, W. (2012), 'Boundary layer stability and Arctic climate change: A feedback study using EC-Earth', *Climate dynamics* **39**(11), 2659–2673.

Blackburn, M. and Hoskins, B. J. (2013), 'Context and aims of the aqua-planet experiment', *Journal of the Meteorological Society of Japan. Ser. II* **91**, 1–15.

Caballero, R. and Langen, P. L. (2005), 'The dynamic range of poleward energy transport in an atmospheric general circulation model', *Geophysical Research Letters* **32**(2).

Clark, J. P. and Lee, S. (2019), 'The role of the tropically excited arctic warming mechanism on the warm arctic cold continent surface air temperature trend pattern', *Geophysical Research Letters* **46**(14), 8490–8499.

Collins, M., Knutti, R., Arblaster, J., Dufresne, J.-L., Fichefet, T., Friedlingstein, P., Gao, X., Gutowski, W. J., Johns, T., Krinner, G. et al. (2013), Long-term climate change: projections, commitments and irreversibility, *in* 'Climate Change 2013-The Physical Science Basis: Contribution of Working Group I to the Fifth

Assessment Report of the Intergovernmental Panel on Climate Change', Cambridge University Press, pp. 1029–1136.

Colman, R., McAvaney, B., Fraser, J. and Power, S. (1994), 'Annual mean meridional energy transport modelled by a general circulation model for present and 2× CO 2 equilibrium climates', *Climate dynamics* **10**(4), 221–229.

ERA-40 Atlas (n.d.), https://sites.ecmwf.int/era/40-atlas/docs/index.html. Accessed: 2020-11-08.

Feldl, N., Anderson, B. T. and Bordoni, S. (2017), 'Atmospheric eddies mediate lapse rate feedback and Arctic amplification', *Journal of Climate* **30**(22), 9213–9224.

Flournoy, M. D., Feldstein, S. B., Lee, S. and Clothiaux, E. E. (2016), 'Exploring the tropically excited arctic warming mechanism with station data: Links between tropical convection and arctic downward infrared radiation', *Journal of the Atmospheric Sciences* **73**(3), 1143–1158.

GISTEMP Team (2020), 'GISS Surface Temperature Analysis (GISTEMP), version 4. NASA Goddard Institute for Space Studies', data.giss.nasa.gov/gistemp/. Accessed: 2021-01-06.

Graversen, R. G. and Wang, M. (2009), 'Polar amplification in a coupled climate model with locked albedo', *Climate Dynamics* **33**(5), 629–643.

Hall, A. (2004), 'The role of surface albedo feedback in climate', *Journal of Climate* **17**(7), 1550–1568.

Hansen, J., Ruedy, R., Sato, M. and Lo, K. (2010), 'Global surface temperature change', *Reviews of Geophysics* **48**(4).

Hartmann, D. L. (2016), Chapter 6 - Atmospheric General Circulation and Climate,

in D. L. Hartmann, ed., 'Global Physical Climatology (Second Edition)', second edition edn, Elsevier, Boston, pp. 159 – 193.

Held, I. M. and Soden, B. J. (2006), 'Robust responses of the hydrological cycle to global warming', *Journal of climate* **19**(21), 5686–5699.

Holton, J. R. (1973), 'An introduction to dynamic meteorology', *American Journal of Physics* **41**(5), 752–754.

HSU, P.-C., TSOU, C.-H., HSU, H.-H. and CHEN, J.-H. (2009), 'Eddy Energy along the Tropical Storm Track in Association with ENSO', *Journal of the Meteorological Society of Japan. Ser. II* **87**(4), 687–704.

Hu, Y., Huang, H. and Zhou, C. (2018), 'Widening and weakening of the Hadley circulation under global warming', *Science Bulletin* **63**(10), 640–644.

Hwang, Y.-T., Frierson, D. M. and Kay, J. E. (2011), 'Coupling between Arctic feedbacks and changes in poleward energy transport', *Geophysical Research Letters* **38**(17).

IFS Cycle 43 r3 (n.d.), https://www.ecmwf.int/en/forecasts/documentation/evolution-ifs/cycles/cycle-43r3. Accessed: 2020-11-02.

Jackson, L., Kahana, R., Graham, T., Ringer, M., Woollings, T., Mecking, J. and Wood, R. (2015), 'Global and European climate impacts of a slowdown of the AMOC in a high resolution GCM', *Climate dynamics* **45**(11-12), 3299–3316.

Laurila, T. K., Sinclair, V. A. and Gregow, H. (2020), 'The Extratropical transition of hurricane Debby (1982) and the subsequent development of an intense windstorm over Finland', *Monthly weather review* **148**(1), 377–401.

Lee, S. (2014), 'A theory for polar amplification from a general circulation perspective', *Asia-Pacific Journal of Atmospheric Sciences* **50**(1), 31–43.

Levine, X. J. and Schneider, T. (2011), 'Response of the Hadley circulation to climate change in an aquaplanet GCM coupled to a simple representation of ocean heat transport', *Journal of the Atmospheric Sciences* **68**(4), 769–783.

Liu, J., Curry, J. A., Wang, H., Song, M. and Horton, R. M. (2012), 'Impact of declining Arctic sea ice on winter snowfall', *Proceedings of the National Academy of Sciences* **109**(11), 4074–4079.

Mak, M.-K. (1969), 'Laterally Driven Stochastic Motions in the Tropics', *Journal of the Atmospheric Sciences* **26**(1), 41–64.

Manabe, S. and Wetherald, R. T. (1980), 'On the distribution of climate change resulting from an increase in CO2 content of the atmosphere', *Journal of the Atmospheric Sciences* **37**(1), 99–118.

Masson-Delmotte, V., Schulz, M., Abe-Ouchi, A., Beer, J., Ganopolski, A., Rouco, J. G., Jansen, E., Lambeck, K., Luterbacher, J., Naish, T. et al. (2013), 'Information from Paleoclimate Archives In: Climate Change 2013: The Physical Science Basis Contribution of Working Group I to the Fifth Assessment Report of the Intergovernmental Panel on Climate Change ed TF Stocker et al', *Cambridge, United Kingdom and New York, NY, USA* .

Mayer, M. and Haimberger, L. (2012), 'Poleward atmospheric energy transports and their variability as evaluated from ECMWF reanalysis data', *Journal of climate* **25**(2), 734–752.

Meleshko, V. P., Johannessen, O. M., Baidin, A. V., Pavlova, T. V. and Govorkova, V. A. (2016), 'Arctic amplification: does it impact the polar jet stream?', *Tellus A: Dynamic Meteorology and Oceanography* **68**(1), 32330.

Mori, M., Watanabe, M., Shiogama, H., Inoue, J. and Kimoto, M. (2014), 'Robust

Arctic sea-ice influence on the frequent Eurasian cold winters in past decades', *Nature Geoscience* **7**(12), 869–873.

Neale, R. B. and Hoskins, B. J. (2000), 'A standard test for AGCMs including their physical parametrizations: I: The proposal', *Atmospheric Science Letters* **1**(2), 101–107.

O'Gorman, P. (n.d.), 'The general circulation of the atmosphere and climate change', http://pog.mit.edu/src/GeneralCirculationNotes_withFigs.pdf. Accessed: 2020-11-08.

Oliver, J. E. (2008), *Encyclopedia of world climatology*, Springer Science & Business Media.

Oort, A. H. (1971), 'The observed annual cycle in the meridional transport of atmospheric energy', *Journal of the Atmospheric Sciences* **28**(3), 325–339.

Oort, A. H. and Peixóto, J. P. (1983), Global angular momentum and energy balance requirements from observations, *in* 'Advances in Geophysics', Vol. 25, Elsevier, pp. 355–490.

Oort, A. H. and Rasmusson, E. M. (1970), 'On the annual variation of the monthly mean meridional circulation', *Monthly Weather Review* **98**(6), 423–442.

OpenIFS Documentation (n.d.), https://confluence.ecmwf.int/display/OIFS/OpenIFS+Home. Accessed: 2020-11-02.

O'Gorman, P. A. and Schneider, T. (2008), 'The hydrological cycle over a wide range of climates simulated with an idealized GCM', *Journal of Climate* **21**(15), 3815–3832.

Pachauri, R. K., Allen, M. R., Barros, V. R., Broome, J., Cramer, W., Christ, R., Church, J. A., Clarke, L., Dahe, Q., Dasgupta, P. et al. (2014), *Climate change*

2014: synthesis report. Contribution of Working Groups I, II and III to the fifth assessment report of the Intergovernmental Panel on Climate Change, IPCC.

Peixoto, J. P. and Oort, A. H. (1992), *Physics of climate*, AIP-Press, US.

Pithan, F. and Mauritsen, T. (2014), 'Arctic amplification dominated by temperature feedbacks in contemporary climate models', *Nature Geoscience* **7**(3), 181–184.

Post, E., Bhatt, U. S., Bitz, C. M., Brodie, J. F., Fulton, T. L., Hebblewhite, M., Kerby, J., Kutz, S. J., Stirling, I. and Walker, D. A. (2013), 'Ecological consequences of sea-ice decline', *Science* **341**(6145), 519–524.

Rantanen, M., Räisänen, J., Sinclair, V. A., Lento, J. and Järvinen, H. (2020), 'The extratropical transition of Hurricane Ophelia (2017) as diagnosed with a generalized omega equation and vorticity equation', *Tellus A: Dynamic Meteorology and Oceanography* **72**(1), 1–26.

Screen, J. A. and Simmonds, I. (2010), 'The central role of diminishing sea ice in recent Arctic temperature amplification', *Nature* **464**(7293), 1334–1337.

Serreze, M. C. and Barry, R. G. (2011), 'Processes and impacts of Arctic amplification: A research synthesis', *Global and planetary change* **77**(1-2), 85–96.

Sévellec, F., Fedorov, A. V. and Liu, W. (2017), 'Arctic sea-ice decline weakens the Atlantic meridional overturning circulation', *Nature Climate Change* **7**(8), 604–610.

Shaw, T., Baldwin, M., Barnes, E. A., Caballero, R., Garfinkel, C., Hwang, Y.-T., Li, C., O'Gorman, P., Rivière, G., Simpson, I. et al. (2016), 'Storm track processes and the opposing influences of climate change', *Nature Geoscience* **9**(9), 656–664.

Sinclair, V., Rantanen, M., Haapanala, P., Räisänen, J., Järvinen, H. et al. (2020),

'The characteristics and structure of extra-tropical cyclones in a warmer climate', *Weather and Climate Dynamics* **1**(1), 1–25.

Singarayer, J. S., Bamber, J. L. and Valdes, P. J. (2006), 'Twenty-first-century climate impacts from a declining Arctic sea ice cover', *Journal of Climate* **19**(7), 1109–1125.

Smith, D. M., Dunstone, N. J., Scaife, A. A., Fiedler, E. K., Copsey, D. and Hardiman, S. C. (2017), 'Atmospheric response to Arctic and Antarctic sea ice: The importance of ocean–atmosphere coupling and the background state', *Journal of Climate* **30**(12), 4547–4565.

Smith, D. M., Screen, J. A., Deser, C., Cohen, J., Fyfe, J. C., García-Serrano, J., Jung, T., Kattsov, V., Matei, D., Msadek, R. et al. (2019), 'The Polar Amplification Model Intercomparison Project (PAMIP) contribution to CMIP6: Investigating the causes and consequences of polar amplification', *Geoscientific Model Development* **12**(3), 1139–1164.

Stocker, T. (2011), *Introduction to climate modelling*, Springer Science & Business Media.

Stott, L., Poulsen, C., Lund, S. and Thunell, R. (2002), 'Super ENSO and global climate oscillations at millennial time scales', *Science* **297**(5579), 222–226.

Szépszó, G., Sinclair, V. and Carver, G. (2019), 'Using the ECMWF OpenIFS model and state-of-the-art training techniques in meteorological education', *Advances in Science & Research* **16**.

Vallis, G. K., Zurita-Gotor, P., Cairns, C. and Kidston, J. (2015), 'Response of the large-scale structure of the atmosphere to global warming', *Quarterly Journal of the Royal Meteorological Society* **141**(690), 1479–1501.

Visser, K., Thunell, R. and Stott, L. (2003), 'Magnitude and timing of temperature change in the Indo-Pacific warm pool during deglaciation', *Nature* **421**(6919), 152–155.

Webster, P. J. (2004), *The Elementary Hadley Circulation*, Springer Netherlands, Dordrecht, pp. 9–60.

Yuval, J. and Kaspi, Y. (2020), 'Eddy Activity Response to Global Warming–Like Temperature Changes', *Journal of Climate* **33**(4), 1381–1404.

7. Acknowledgements

I would like to express my gratitude to my supervisor Victoria Sinclair for guiding me through the work of this thesis and for the expertise and support I was served with. I am deeply grateful for being part of atmospheric dynamics research at the University of Helsinki from which I gained valuable knowledge that will be important in my future academic career. I also would like to thank to my family for supporting me in my studies and making me available to follow Meteorology studies outside my home country. Köszönöm apa és anya! I am also thankful for the University of Helsinki to accept me as an international student and to provide me a stimulating environment where I could broaden my knowledge. Kiitos Suomi ja Helsingin Yliopisto, että minä sain opiskella täällä ja viettää upeaa aikaa opintojeni aikana. I also would like to thank my friend, Alex for supporting me in writing this thesis in LaTeX. In addition, I shall thank for my fellow Meteorology students for the precious time we have spent together during our studies.

8. Appendix A

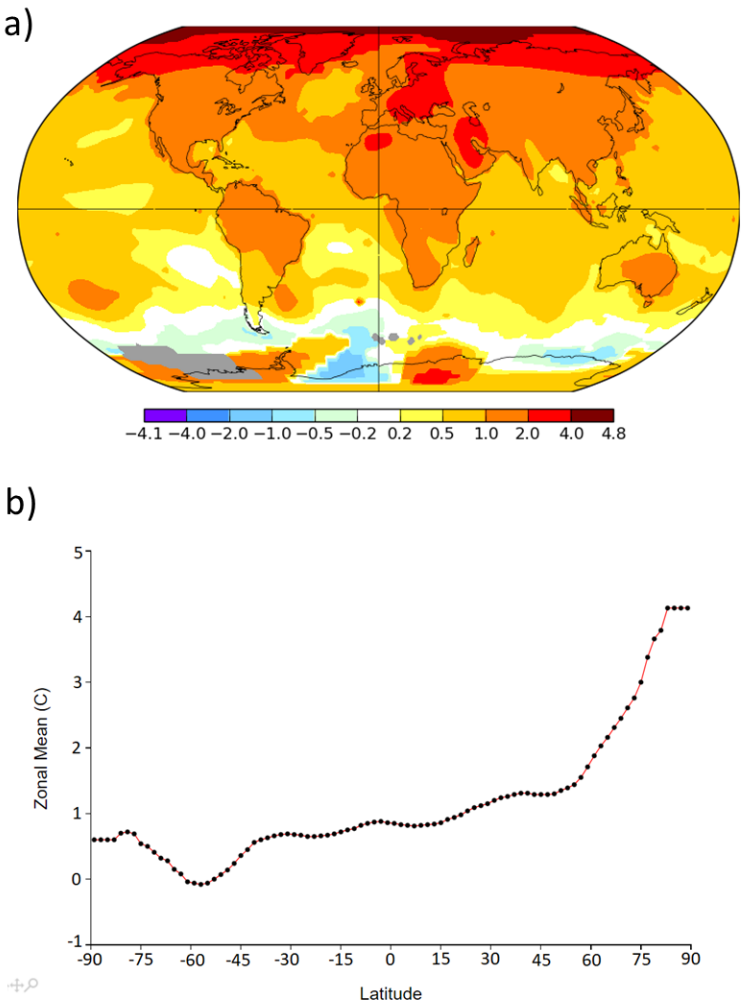

Figure 8.1: Annual surface temperature changes between 1970 and 2019 based on NASA GISS analysis showing the a) global distribution of surface temperature changes and b) the zonal mean surface temperature changes in °C. Figure adopted from (GISTEMP Team, 2020).

9. Appendix B

a)

$$T(QObs)[°C] = \begin{cases} \frac{\Delta T}{2}\left(2 - \sin^2\left(\frac{3\phi}{2}\right) - \sin^4\left(\frac{3\phi}{2}\right)\right); -\frac{\pi}{3} < \phi < \frac{\pi}{3} \\ 0 \quad ; \text{ otherwise} \end{cases}$$

$$\Delta T = 27°C$$

b)

$$T(PA)[°C] = \begin{cases} 5 + \frac{\Delta T}{2}\left(2 - \sin^2\left(\frac{3\phi}{2}\right) - \sin^4\left(\frac{3\phi}{2}\right)\right); -\frac{\pi}{3} < \phi < \frac{\pi}{3} \\ 5 \quad ; \text{ otherwise} \end{cases}$$

$$\Delta T = 22°C$$

Figure 9.1: Geometric equations describing the hemispherically symmetric zonal mean SST pattern of the CTRL and the PA simulation. The visualised equations can be followed by Fig.3.1. Equation a) describes the SST field of the CTRL simulation with $\Delta T = 27°C$. Equation b) gives information about the SST field of the PA simulation with $\Delta T = 22°C$. ΔT is equal with the temperature difference between the equator and the pole.

10. Appendix C

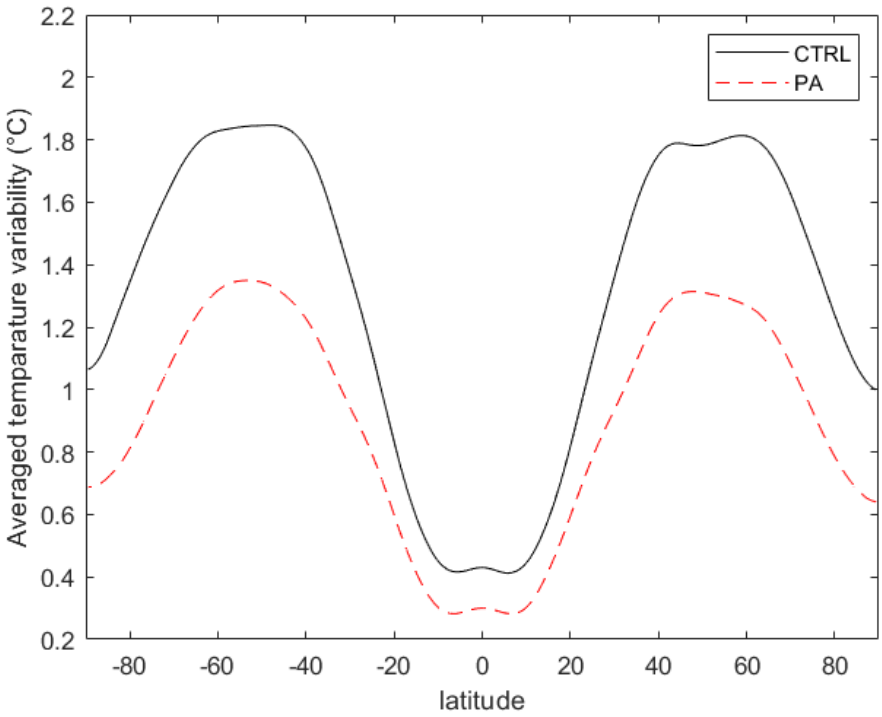

Figure 10.1: Vertical and zonal mean standard deviation of day-to-day temperature ($\sqrt{\left[\bar{T'^2}\right]}$) in the CTRL (black line) and in the PA simulation (dashed red line) expressed in °C.

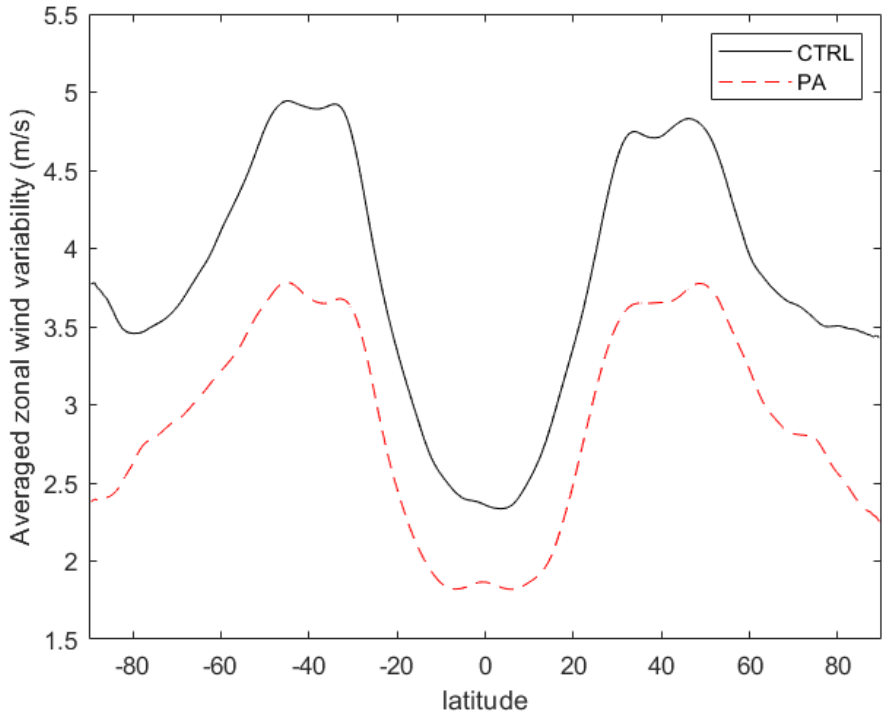

Figure 10.2: Vertical and zonal mean standard deviation of day-to-day zonal wind (i.e. u-wind) ($\sqrt{\left[\bar{u'^2}\right]}$) in the CTRL (black line) and in the PA simulation (dashed red line) expressed in $m\ s^{-1}$.

11. Appendix D

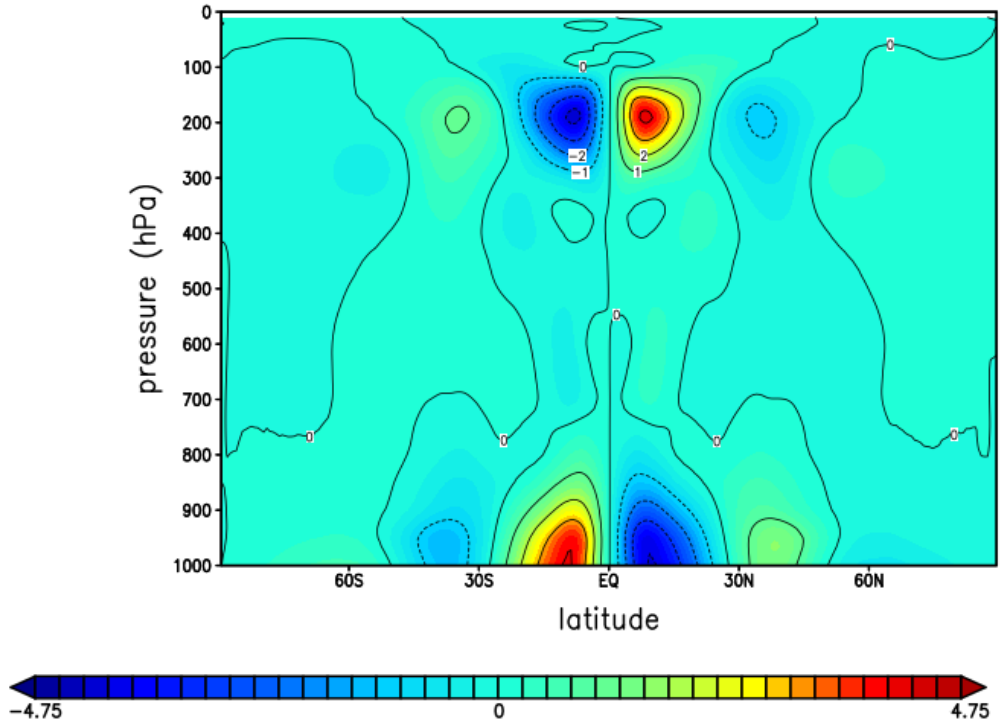

Figure 11.1: Vertical cross-section of the zonal and time mean meridional wind ($m\ s^{-1}$) of the CTRL aqua planet simulation.

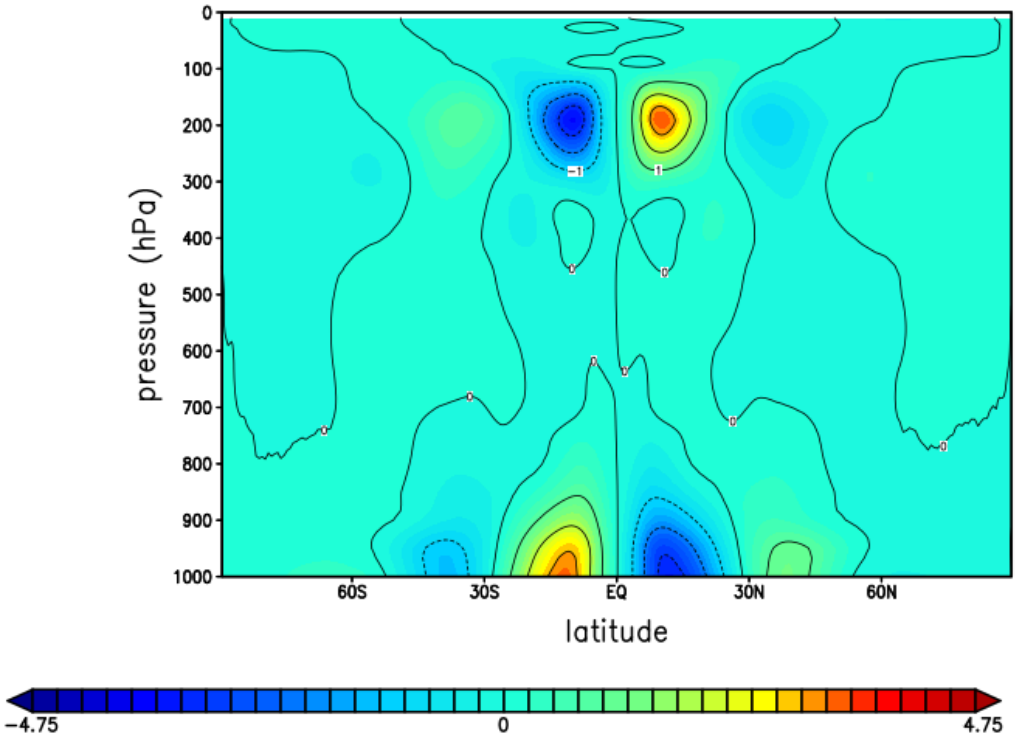

Figure 11.2: Vertical cross-section of the zonal and time mean meridional wind ($m\ s^{-1}$) of the PA aqua planet simulation.

12. Appendix E

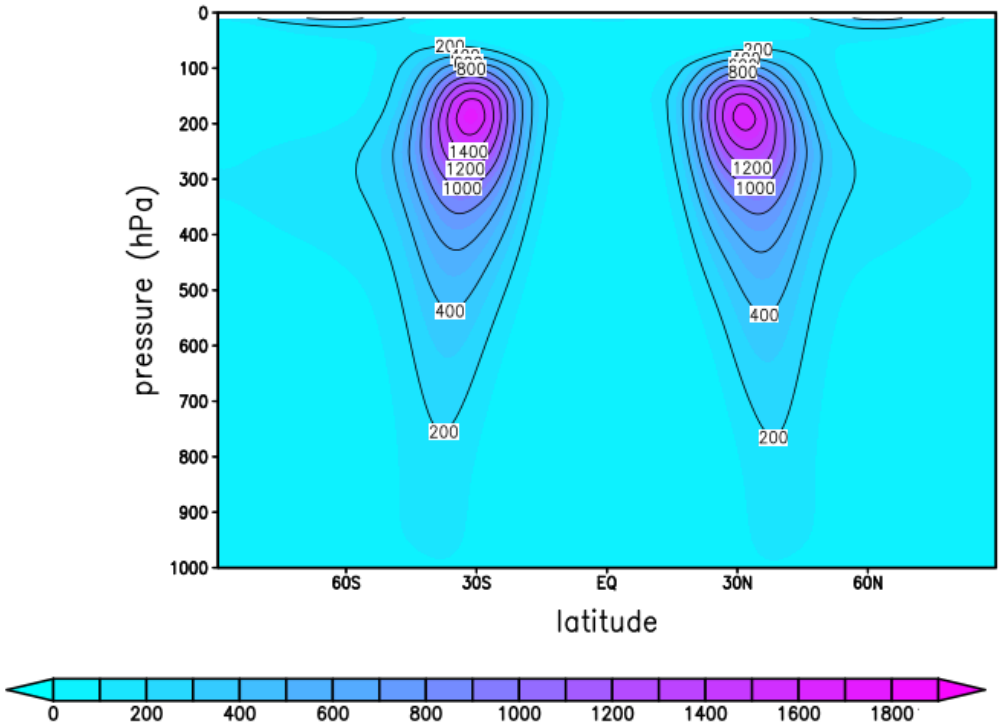

Figure 12.1: Mean kinetic energy content of the atmosphere ($J\ kg^{-1}$) in the CTRL aqua planet simulation.

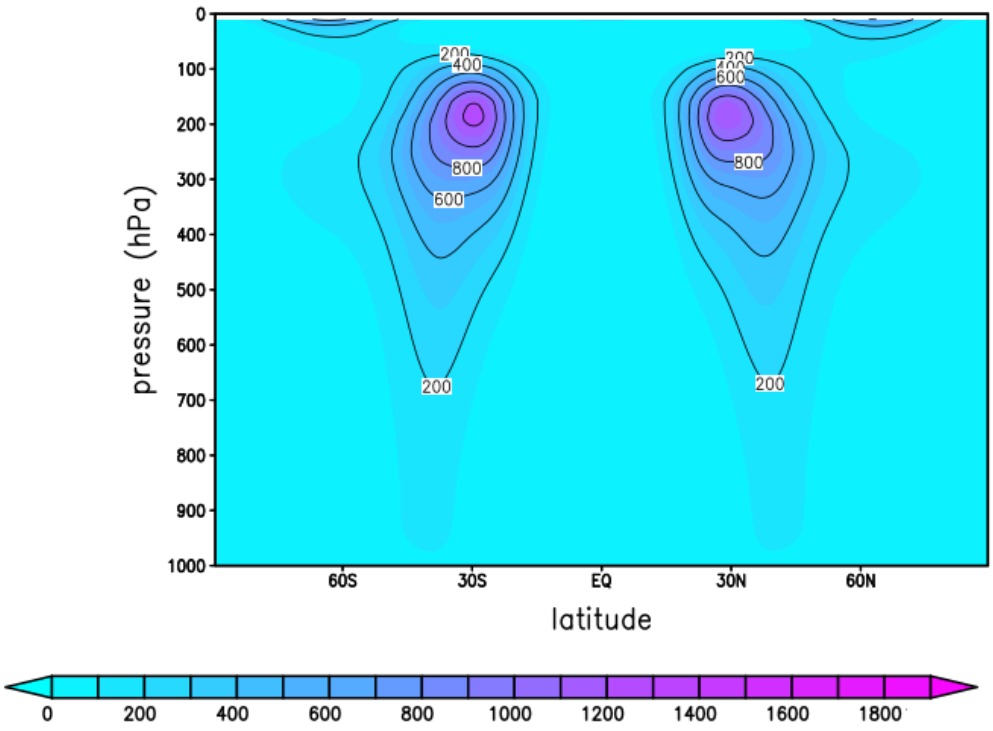

Figure 12.2: Mean kinetic energy content of the atmosphere ($J\ kg^{-1}$) in the PA aqua planet simulation.

13. Appendix F

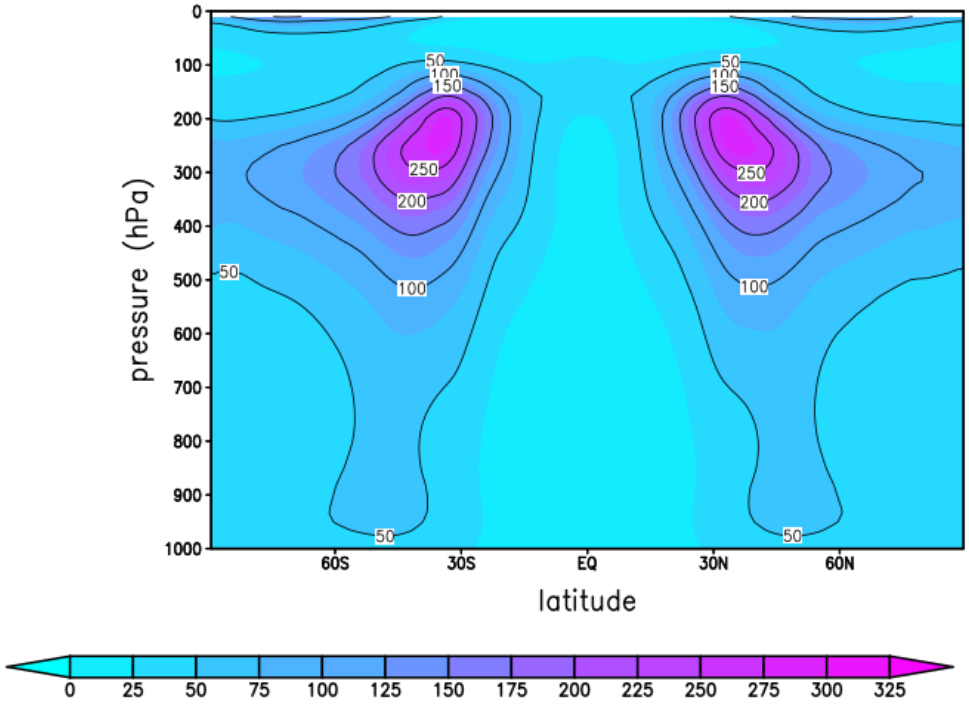

Figure 13.1: Transient eddy kinetic energy content of the atmosphere ($J\ kg^{-1}$) in the CTRL aqua planet simulation.

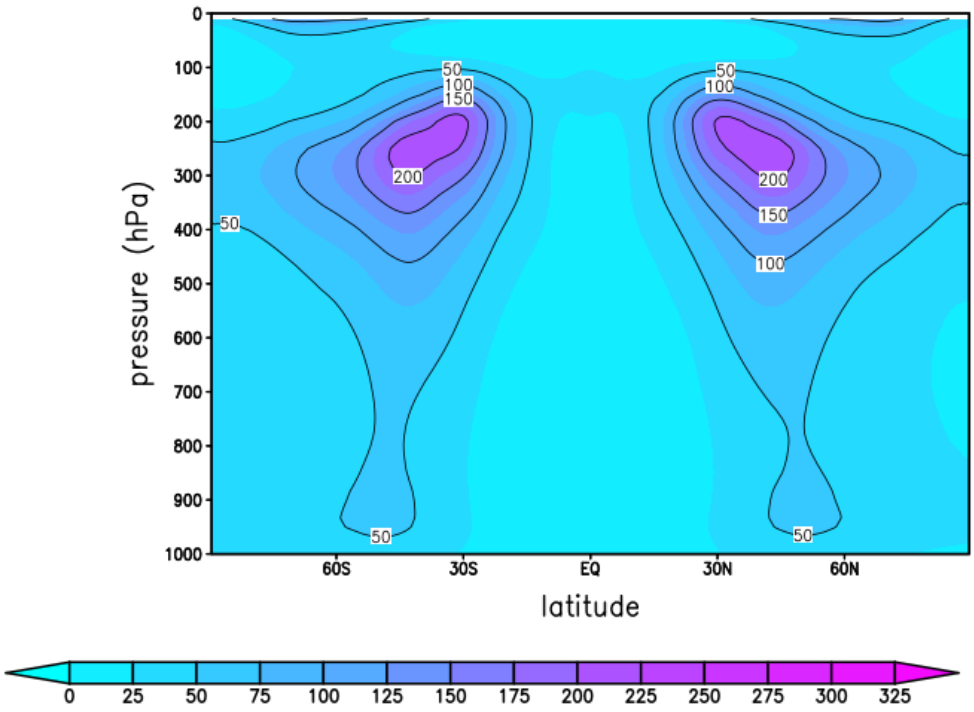

Figure 13.2: Transient eddy kinetic energy content of the atmosphere ($J\ kg^{-1}$) in the PA aqua planet simulation.